Photon strength functions, level densities, and isomeric ratio in ^{168}Er from the radiative neutron capture measured at the DANCE facility

I. Knapová,[1,*] A. Couture,[2] C. Fry,[2] J. Kvasil,[1] M. Krtička,[1] V. O. Nesterenko,[3,4] J. M. O'Donnell,[2] C. J. Prokop,[2] G. Rusev,[2] J. L. Ullmann,[2] and S. Valenta[1]

[1]*Faculty of Mathematics and Physics, Charles University, 180 00 Prague, Czech Republic*
[2]*Los Alamos National Laboratory, Los Alamos, New Mexico 87545, USA*
[3]*Laboratory of Theoretical Physics, Joint Institute for Nuclear Research, Dubna, Moscow Region 141980, Russia*
[4]*State University "Dubna", Dubna, Moscow Region 141980, Russia*

(Received 1 September 2022; revised 2 March 2023; accepted 21 March 2023; published 18 April 2023)

Background: The statistical approach is usually applied for the description of electromagnetic decay of the nucleus with the exception of the lowest excitation energies as well as for the calculation of the interaction of photons with nuclei, in particular the reaction cross sections. This concept employs nuclear level density (NLD) and photon strength functions (PSFs).

Purpose: While PSFs and NLD of some well-deformed rare-earth nuclei were measured by several methods, sometimes with conflicting results, the PSFs of ^{168}Er were addressed only by (γ, γ') experiments. On the other hand, the low-lying levels of ^{168}Er are well studied, including the isomeric state at 1094 keV, which enables various tests of the statistical approach.

Methods: The γ rays following radiative neutron capture on a ^{167}Er sample were measured with the highly segmented γ-ray calorimeter Detector for Advanced Neutron Capture Experiments at the Los Alamos Neutron Science Center. The γ-ray energy spectra for different multiplicities (multistep cascade, or MSC, spectra) were gathered for many s-wave resonances of both possible spins. Moreover, we were able to detect the decay of the short-lived isomer and deduce the isomeric ratio for a few resonances.

Results: Analysis of the MSC spectra within the statistical model enabled us to draw conclusions about dipole PSFs, in particular on the properties of the scissors mode, and NLD. The spectra can be well reproduced with phenomenological PSFs models but not with any of several models based on quasiparticle random-phase approximation (QRPA) calculations with different interactions. We showed that nonstatistical effects in feeding of the isomeric state play a role up to excitation energies of at least about 2 MeV.

Conclusions: Deduced parameters of the scissors mode were found to be similar to those of neighbor well-deformed even-even Gd and Dy nuclei. Models like that of Kadmenskij, Markushev, and Furman (KMF) or like the modified generalized Lorentzian (MGLO) model provide a good description of experimental spectra. In contrast to several previous analyses of well-deformed rare-earth isotopes, we were able to match the experimental isomeric ratio with statistical model simulations.

DOI: 10.1103/PhysRevC.107.044313

I. INTRODUCTION

In medium- and heavy-mass nuclei complete spectroscopic information can be experimentally obtained only for levels at the lowest excitation energies, below 1.5–2 MeV in even-even nuclei. These limitations originate mainly from the rapid increase of the nuclear level density (NLD) with excitation energy. The γ decay of these nuclei at higher excitation energies is then usually described using the statistical model in terms of the NLD and a set of photon strength functions (PSFs) for different transition types. These quantities are essential for calculations of cross sections in all nuclear reactions involving photons, which play an important role especially in nuclear astrophysics [1,2] and in the development of advanced nuclear reactors [3].

There are many models of both the PSFs and NLD available in the literature [4,5] and their validation as well as obtaining further information on the properties of these quantities is important. The two PSF features that strongly influence the γ decay of neutron resonances in well-deformed nuclei are the energy dependence of the giant electric dipole resonance (GEDR) low-energy tail and the collective $M1$ excitation known as the scissors mode (SM) [6,7].

The use of the statistical approach might not be fully appropriate in the region where we start to miss information on low-lying levels and where structural effects still could play a significant role. Nevertheless, the validity of the approach is difficult to test in this region. Although analyses of neutron capture data [8–10] and the so-called Oslo method [11–13] assume its applicability and do not observe significant deviations, the data from (γ, γ') reaction cast some doubts; see discussion and Fig. 43 in Ref. [14].

*Corresponding author: knapova@ipnp.mff.cuni.cz

In this paper, we investigate the applicability of the statistical model in this region using ^{168}Er, perhaps the best studied well-deformed rare-earth nucleus at low excitation energies. This isotope attracted great attention from both the experimental and theoretical sides until the 1990s. Most notably, in 1981 Davidson *et al.* [15] combined high-resolution bent crystal gamma and beta spectroscopy from the ILL with resonance and average resonance capture measurements taken at the BNL reactor. Later, Jungclaus *et al.* [16] carefully examined the previous claims about the completeness of the decay scheme using another high-resolution coincidence measurement of the γ cascades following the thermal neutron capture. Their conclusion is that the decay scheme is complete up to 2 and 2.2 MeV for positive and negative parity levels, respectively; for details see [16] and references therein. Their findings are, among others, reflected in the latest ENSDF evaluation [17].

Besides the supposedly complete decay scheme up to at least 2 MeV, ^{168}Er exhibits another feature: the presence of an isomer with a half-life $T_{1/2} = 109$ ns at excitation energy of 1094 keV [17]. Study of population of this isomer should reveal further information on the validity of the statistical model. In the simulations, the so-called *critical energy* $E_{\rm crit}$ divides the excitation energies into two domains: the low excitation energies, where the information about levels is taken from experimental data or evaluations, and the region above this interval, where the description by NLD and PSFs is used. In previous resonant neutron capture studies of short-lived isomers in rare-earth nuclei, with half-lives of tens to hundreds of ns, the deduced experimental populations were considerably higher than the simulated ones; see Hf results from the Karlsruhe Total Absorbtion Calorimeter [18] and Lu from CIRENE [19] and DANCE [20]. Reference [20] also pointed out the importance of treatment of the low-lying decay scheme on the isomeric ratio $R_{\rm iso}$. The authors observed an increase (by about a fifth) in $R_{\rm iso}$ predicted from the statistical model simulations when changing $E_{\rm crit}$ from 1.4 to 1.9 MeV.

Important information on PSFs and NLD as well as population of the isomeric state can be obtained from the analysis of coincident γ-ray spectra measured in the decay of isolated neutron resonances. These spectra were measured with the Detector for Advanced Neutron Capture Experiments (DANCE) [21,22] installed at the pulsed neutron beam at Los Alamos Neutron Science Center (LANSCE) [23,24] at Los Alamos National Laboratory.

In Sec. II we describe the experimental techniques to measure the spectra with the DANCE calorimeter and in Sec. III the modeling of the statistical γ cascades. Information about the PSFs and NLD that can be extracted from the measured spectra is then presented in Sec. IV and the findings are compared to available data in Sec. V. The results related to the population of the isomeric state are then given in Sec. VI and the summary is provided in Sec. VII.

II. EXPERIMENT AND DATA REDUCTION

A. Experimental setup

The experiment was performed at the moderated spallation neutron source LANSCE [23,24], which produces a white spectrum of neutrons with energies ranging from subthermal to several MeV with a repetition rate of 20 Hz. The neutrons enter the flight path 14 at the Manuel Lujan Jr. Neutron Scattering Center and at 20 m from the spallation target they impinge on the Er sample located in the center of the DANCE detector [21,22], an array of 160 BaF_2 scintillation crystals, which covers a solid angle of $\simeq 3.5\pi$. The 9921QB photomultiplier is attached to each DANCE crystal forming 160 independent detection modules. Each module serves as a γ spectrometer. A 6-cm-thick ^{6}LiH shell is placed between the sample and the BaF_2 crystals in order to reduce the scattered neutron flux. In addition to the BaF_2 crystals, the experimental setup includes beam monitors to validate the stability of the neutron flux. A comprehensive description of the experimental setup and initial data processing can be found in Refs. [21,22,25,26].

The ^{167}Er sample, enriched to 91.5% with other Er isotopes dominating the composition, was prepared at Oak Ridge National Laboratory as self-supporting, $\frac{1}{4} \times \frac{1}{4}$ inch metal foil weighting 20.1 mg.

B. Initial data reduction

The signals from individual modules are processed using 14-bit CAEN VC1730 digitizers with 16 channels, running at 500 megasamples per second [26]. The scintillation light emitted by the BaF_2 crystals is formed by slow ($\tau \approx 600$ ns) and fast ($\tau \approx 600$ ps) components. Fast (12 ns) and slow (1 μs) integrals as well as a waveform snippet of the first 80 ns were acquired for each BaF_2 event. The fast-to-slow ratio is used to discriminate γ rays against the α background from Ra, the chemical homologue of Ba present in the crystals. The spectrum of α particles is then used for run-by-run energy calibration, together with ancillary measurements of γ-ray sources (^{88}Y, ^{22}Na). A common software threshold for deposited γ-ray energy of 200 keV was used for all modules.

All signals arriving within a 6 ns coincidence window were considered to belong to the same event, which is characterized by the corresponding neutron energy, obtained by the time-of-flight technique, and number of firing crystals with the energy deposited in each of them. Due to Compton scattering, a single γ ray often deposits its energy in several, usually neighboring crystals. All adjacent crystals that fired during an event are therefore combined into a *cluster* and the number of clusters that were hit is labeled as the *cluster multiplicity* M. The cluster-related observables are used in this work as the cluster multiplicity is closer to the emitted γ multiplicity than the crystal multiplicity and some features of the decay are more pronounced in the respective spectra. When a module of DANCE triggers a channel in the data acquisition system, the charge integral of the triggered channel is recorded for 1 μs, and during this time the module cannot trigger again. This effect leads to dead time that is monitored and the information about busy modules is available during further analysis.

Only events corresponding to well-resolved resonances,[1] identified from the time-of-flight spectrum, with sufficient

[1]For analysis of $R_{\rm iso}$ also one off-resonance region was used.

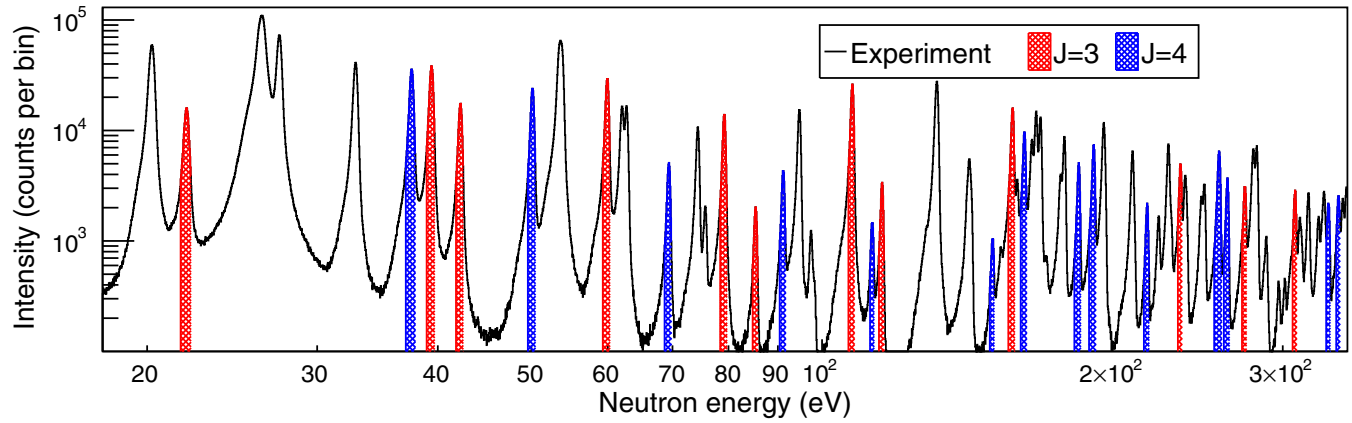

FIG. 1. Experimental time-of-flight spectrum after transformation to neutron energy for events with $M = 2$–6 and $E_\Sigma = 7$–8 MeV. The hatched intervals of a given spin correspond to neutron energy regions used in the analysis. There are 2500 logarithmic bins per decade.

statistics were analyzed; see Fig. 1. The spins of these resonances are unambiguous [27,28]. Special care was taken to avoid the neutron energy domains with, on average, too high number of busy modules, effectively preventing us to gather information from the strongest resonances at low neutron energies. It was verified that the spectra from these regions are distorted [29].

C. Sum-energy and multistep cascade spectra

Spectra of sums of deposited γ-ray energies within an event, hereafter called the *sum-energy* spectra, are shown in Fig. 2 for two resonances of each spin and $M = 2$–5. The spectra are normalized to the same total number of events

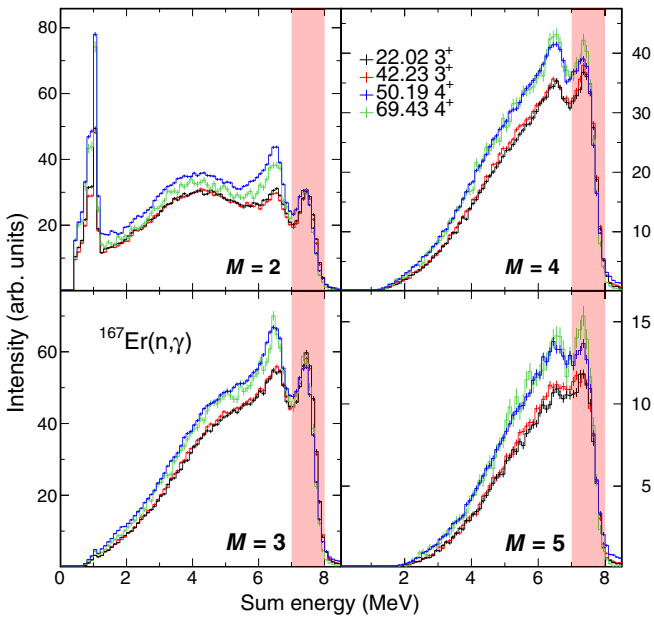

FIG. 2. Experimental background-subtracted sum-energy spectra for two $J^\pi = 3^+$ and two 4^+ neutron resonances and multiplicities $M = 2$–5. The red band illustrates the interval $E_\Sigma = 7$–8 MeV used to construct the MSC spectra.

for $M = 2$–6 in the sum-energy range $E_\Sigma = 7$–8 MeV, which corresponds (within the detector resolution) to the reaction Q value given practically by the neutron separation energy $S_n = 7.771$ MeV [17]. For the resonances under consideration ($E_n < 1$ keV), the incident neutron energy does not significantly impact the sum-energy.

The sum-energy spectrum from the ^{167}Er(n, γ) reaction consists of (i) the full-energy peak at $E_\Sigma \approx S_n$, corresponding to events where all the energy of a γ cascade was detected, (ii) a peak at $E_\Sigma \approx 6.5$ MeV from the cascades feeding the isomer at 1.094 MeV, (iii) a peak at $E_\Sigma \approx 1.1$ MeV in $M = 2$ from the isomeric decay, and (iv) lower-energy tails corresponding to each of these peaks (i)–(iii), originating from events where a part of the γ-ray energy escaped the detection. The vast majority of the cascades going through the isomer are detected as two separate events corresponding to the feeding and the decay, as its $T_{1/2} = 109$ ns is much longer than the adopted coincidence window.

In reality, there is a small background contribution in the sum-energy spectra originating from two different sources. First, signals from natural β radioactivity in the BaF_2 crystals are observed for low M for $E_\Sigma < 3$ MeV. Second, neutrons scattered from the sample and captured in the BaF_2 crystals give a contribution for low M. As two isotopes of Ba have $S_n > 8.5$ MeV, the full-energy peaks from these reactions are above the full-energy peak from the ^{167}Er capture and indicate the level of background. These background contributions were subtracted using the spectra from the neighboring off-resonance regions.

From the events in the $E_\Sigma = 7$–8 MeV range (depicted in Fig. 2 as red bands) we construct the *multistep cascade* (MSC) spectra, which correspond to spectra of individual γ-ray energies deposited within M clusters. Examples of the MSC spectra from individual resonances are shown in Fig. 3. The background subtraction in the MSC spectra was performed analogously to the sum-energy spectra. The presented MSC spectra inherit the normalization of the sum-energy spectra. The bin width of 100 keV was chosen for both aforementioned types of spectra, as it is close to the energy resolution for low γ-ray energies. To facilitate the comparison of experimental data with model predictions we constructed the *mean*

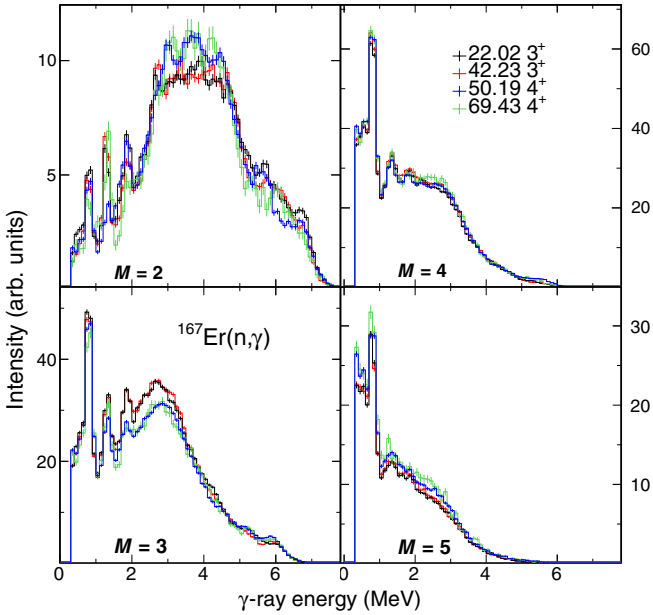

FIG. 3. Experimental background-subtracted MSC spectra for two $J^\pi = 3^+$ and two 4^+ neutron resonances and multiplicities $M =$ 2–5.

experimental MSC spectra from 12 resonances with $J^\pi = 3^+$ and 15 resonances with $J^\pi = 4^+$. In accord with Refs. [10,30], we computed the mean experimental intensity $I_{\rm exp}$ and the fluctuation of the experimental intensity $\phi_{\rm exp}$ for each bin using a maximum likelihood fit considering the experimental uncertainties. In Figs. 6–9 the uncertainty of $I_{\rm exp}$ is represented by a full rectangle, while the $\phi_{\rm exp}$ is displayed as a larger error bar. Further details can be found in Refs. [10,30].

In principle, we could produce the MSC spectra not only for transitions with $E_\Sigma = 7$–8 MeV but also for other ranges. The range of $E_\Sigma \approx 6$–7 MeV could be of special interest as a fraction of the cascades therein corresponds to the decay of neutron resonances to the isomeric state. However, simulations described below indicated that the contribution of the cascades feeding the isomeric state to the total number of detected cascades within $E_\Sigma \approx 6$–7 MeV is smaller than about 20% for each M and the MSC spectra are thus dominated by the cascades ending at the ground state. We can thus hardly learn anything important from this E_Σ range and decided not to present the spectra here. We only note that the comparison of MSC spectra for this lower E_Σ range gives information consistent with that presented in this paper; see Ref. [31].

Spectra for $M = 1$ were not considered in the data analysis as they are often strongly dominated by background. There are virtually no events with $M > 6$ spectra.

D. Determination of isomeric ratio

An interesting feature of ^{168}Er that should allow an additional check of applicability of the statistical model and possibly different PSFs and NLD models is the population of the $J^\pi = 4^-$ K-isomeric state at 1.094 MeV. The isomeric ratio for states with lifetimes of tens to hundreds ns and detectable deexcitation (presence of a γ-ray with $E_\gamma \gtrsim$ 150 keV) is accessible with reasonable accuracy using DANCE, as demonstrated by Denis-Petit *et al.* [20] for isomers of ^{177}Lu.

The half-life of the isomeric state allows detection of its decay separately from, yet in correlation with, the prompt cascade. To determine the isomeric half-life and ratio, we define a *prompt* γ *cascade* in a way to include the cascades feeding the isomer and a *delayed* γ *cascade* mostly corresponding to the isomeric decay. We postulate specific cuts on the event observables in order to flag events as the prompt, delayed, or other γ cascades. The prompt γ cascade events are those with $M = 2$–6 and $E_\Sigma = 5$–8 MeV, while the delayed γ cascade events fall within $E_\Sigma = 0.4$–1.0 MeV. We then construct spectra of the time differences between the delayed and the prompt γ cascades. These spectra are to be fitted by a sum of the isomeric exponential decay and a second exponential describing the accidental coincidences, as not all the cascades falling into the prompt and delayed cuts originate from the isomer-related cascades. The half-life and the number of detected isomeric decays $N_{\rm iso}$ are obtained from the fit [31]. The isomeric ratio is then calculated from $N_{\rm iso}$ as

$$R_{\rm iso} = \frac{N_{\rm iso}}{\varepsilon_{\rm feed}\,\varepsilon_{\rm iso}} \times \frac{\varepsilon_{\rm pr}}{N_{\rm pr}}, \tag{1}$$

where $N_{\rm pr}$ is the number of detected prompts, which is given by a simple experimental counting. The efficiencies are derived from simulations described in Sec. III. The $\varepsilon_{\rm iso}$ is the probability of detecting the isomeric decay as the delayed γ cascade, the $\varepsilon_{\rm pr}$ is the efficiency of detecting any cascade as the prompt γ cascade, and $\varepsilon_{\rm feed}$ corresponds to the probability of detecting a cascade feeding the isomer as the prompt γ cascade.

III. STATISTICAL MODEL SIMULATIONS

The sum-energy and MSC spectra are products of a complicated interplay between the NLD, PSFs, and nontrivial detector response. Consequently, NLD and PSFs cannot be directly extracted from the experimental spectra. We adopted a trial-and-error approach of comparing experimental spectra to their simulated counterparts assuming various models of NLD and PSFs. This allows us to reject many model combinations and select those giving a reasonable agreement with the experiment. In general, the simulations provide any decay-related quantity. From quantities of interest, we check the MSC spectra, the isomeric ratio $R_{\rm iso}$, and the total radiative width Γ_γ for individual models in this work.

A. Algorithms

The γ cascades following resonance neutron capture on ^{167}Er were generated under various assumptions about the NLD and PSFs using the DICEBOX code [32,33]. The response of the DANCE detector, calculated using a Monte Carlo code [25] based on the GEANT4 package [34], was subsequently applied to simulated γ cascades.

In the DICEBOX algorithm, below some critical energy $E_{\rm crit}$, the complete decay scheme is taken from existing experi-

mental data; we adopted those evaluated in Ref. [17]. Above $E_{\rm crit}$ up to the capturing state individual levels and their decay properties are generated using an *a priori* chosen NLD function ρ and PSFs $S^{(XL)}$, where X denotes the type (electric, $X \equiv E$, or magnetic, $X \equiv M$) and L the multipolarity of the transition, $XL = E1$, $M1$, and $E2$. A contribution of higher multipolarities was neglected. The Porter-Thomas (PT) fluctuations [35], as well as the internal electron conversion, are correctly considered in simulations of individual partial radiative widths $\Gamma_{i\gamma f}$; see [10,32,33].

The set of randomly generated levels and their partial radiative widths is called a *nuclear suprarealization* (NS). In reality, decays of various neutron resonances of the same spin and parity differ only in intensities of primary transitions. To mimic this behavior we randomly generate the intensities of primary transitions within a given NS. Each set of primary decay branching intensities within a given NS is denoted as a *nuclear realization* (NR). During the search for appropriate models of PSFs and NLD (in Sec. IV) we typically simulated 2×10^5 cascades in 20 independent NSs with only one NR for each model combination. As indicated in Sec. IV D, this approach seems to be fully justified. The MSC intensities in the individual bins of MSC spectra were obtained in the same way as their experimental counterparts including the normalization.

To check the population of the isomeric state we performed simulations with a broad range of $E_{\rm crit}$ up to 2.418 MeV to include as many experimentally known levels as possible. With the highest adopted $E_{\rm crit}$ there are already 57 tentative, 10 uncertain, and 3 unknown J^π assignments out of 130 levels [17]. This approach is contradictory to our usual method in which we require at maximum a few uncertain properties of the low-lying levels below $E_{\rm crit}$, which would be about 2.0 MeV in ^{168}Er. The tentative J^π assignments were taken as suggested; for the remaining 13 levels, J^π was estimated based on their decay. Nonetheless, after our tests of other possibilities, it turns out that these uncertainties in the adopted level scheme do not have significant influence on our results. A change of $E_{\rm crit}$ between about 2.0 and 2.418 MeV has only a small impact on produced MSC spectra. However, the reproduction of structures clearly visible in $M = 2$ and 3 MSC spectra just below 2 MeV is better with higher $E_{\rm crit}$. As a result, with the exception of the isomeric ratio, we only present simulations with the highest adopted $E_{\rm crit}$.

We stress that the predicted spectra are not sensitive to the absolute values of PSFs if the E_γ-dependent ratios of PSFs for different transition types are kept the same. Therefore we can probe the E_γ dependence of the PSFs and their relative contributions rather than the absolute PSF values. The only quantity obtained from the simulations that depends on the absolute PSF values is the total radiative width Γ_γ.

B. Nuclear level density models

Many NLD models are available in the literature. We tested two different phenomenological models given by closed form formulas: (i) the back-shifted Fermi gas (BSFG) model and (ii) the constant-temperature (CT) model. Each of these models includes adjustable parameters. Two sets of parameters were tested for each model, corresponding to two different parametrizations from the works of von Egidy and Bucurescu [36,37].

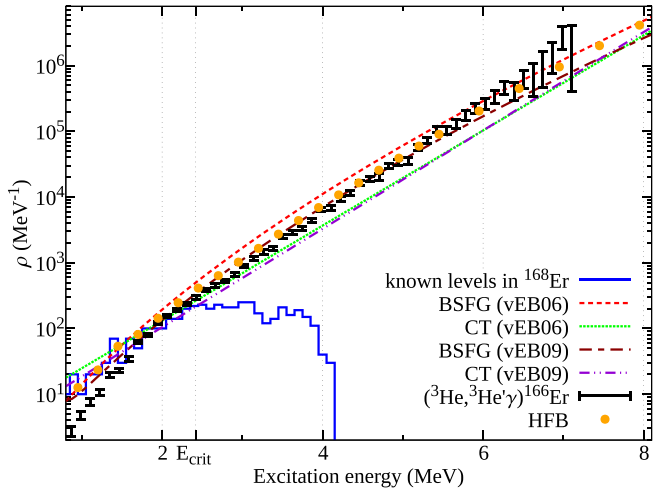

FIG. 4. Level density models of ^{168}Er tested in our simulations, summed over all spins and parities. BSFG and CT models for two different parametrizations (vEB06 from [36] and vEB09 from [37]) are shown together with the HFB calculations [41]. The experimental NLD data from (^{3}He,^{3} He$'\gamma$)^{166}Er were extracted by the Oslo method [12] The known levels are taken from the ENSDF evaluation [17].

In the majority of the simulations, we assumed no parity dependence of the NLD above $E_{\rm crit}$. However, we also tested the influence of a possible parity dependence using the formula and parameters from Ref. [38], where the parity asymmetry disappears around 3 MeV. We further tested the effect of the even-odd staggering in the spin distribution of even-even nuclei in the form presented in Ref. [39]. The staggering was assumed to linearly decrease with excitation energy and vanish at 4.0 MeV.

Furthermore, we tested the NLD based on the microscopic calculation within the Hartree-Fock-Bogoliubov (HFB) approach plus combinatorial method [5,40,41], labeled as the HFB model below. The calculated level densities usually cannot reproduce the number of low-lying levels and the average neutron resonance spacings, therefore the suggested renormalization was used [41]. The resulting NLD are spin and parity dependent and exhibit a much wider spin distribution than all the above-mentioned models, with the even-odd staggering persisting up to energies near S_n.

The energy dependence of tested NLD models is shown in Fig. 4 together with the Oslo data for ^{166}Er [12]. Note that partial NLD of all tested models matches the s-wave resonance spacing [27].

C. Photon strength function models

The γ decay of neutron resonances is dominated by dipole transitions. The tested models of dipole PSFs are described below. In the simulations, we also consider $E2$ transitions, but we verified they play a negligible role in the statistical decay of the nucleus. In all model combinations presented below

we used the single-particle model of $E2$ PSF, $S^{(E2)} = 1 \times 10^{-11}$ MeV^{-5}.

1. Electric dipole PSF

Electric dipole ($E1$) transitions play a major role for energies above S_n due to the presence of the GEDR. It is widely assumed the $S^{(E1)}$ at these energies for axially deformed nuclei is consistent with the sum of two Lorentzian terms that form the standard Lorentzian (SLO) model [5]. The GEDR parameters are usually deduced from a fit of the (γ, xn) data. We used parametrizations based on natEr data. In practice, there are at least two available GEDR parametrizations of this data, one in the compilation of Dietrich and Berman [42], the other in RIPL-3 [5] and a recent review [43]; the latter will be referred to as RIPL-3 below. These two parametrizations significantly differ in the absolute value, but their E_γ dependence is almost identical below S_n. To apply the SLO (or in general any) model to the γ decay, we need to make assumptions about the PSF among the excited states. The so-called Brink hypothesis [44] stating that the PSF depends only on E_γ is invoked for the SLO model.

The validity of the SLO model for the $S^{(E1)}$ below neutron separation energy is highly questionable in well-deformed rare-earth nuclei [9–12] and many different models for this E_γ region were proposed.

We tested several of these models. One of them was proposed by Kadmenskij, Markushev, and Furman (KMF model) [45] for spherical and weakly deformed nuclei. Although there is no theoretical justification for the use of this model in well-deformed nuclei, it is often adopted also in these cases. The KMF model introduced a weak PSF dependence on excitation energy of the final level E_x (or nuclear temperature $T = \sqrt{(E_x - \Delta_P)/a}$, where Δ_P is the pairing correction and a is the NLD parameter; both were taken from [37]), violating the strict form of the Brink hypothesis [44].

A modification of the KMF model, where the temperature was assumed to be constant ($T \approx 0.3$ MeV) was used in several rare-earth isotopes for PSFs extracted from the ^{3}He induced reactions by employing the Oslo method [11,12,46]. This model, denoted as KMF-T, also allows the reproduction of the two-step cascade (TSC) [47] and MSC [9,48] spectra in other rare-earth nuclei.

Further, the GLO model was introduced for spherical nuclei by Chrien [49] to describe the low-energy PSF behavior by the KMF shape while keeping the SLO dependence near the GEDR maxima. This model was later generalized by Kopecky *et al.* [50] for deformed nuclei by adopting an *ad hoc* parameter k, which depends on the nucleus mass. The recommended value of this parameter was based on the requirement to match the total radiative widths Γ_γ of the neutron resonances. As this quantity strongly depends on the NLD model along with the PSFs for other transition types, we treated k as a free parameter in our simulations. This model is known as the enhanced generalized Lorentzian (EGLO) model. The modified generalized Lorentzian (MGLO) model was proposed [48] as an alternative to the EGLO model and employs the same parameter k. MGLO exhibits a significantly smaller preference for low-energy transitions compared to the EGLO model and it provided a good agreement with the MSC spectra for Gd and Dy isotopes [8–10,48]. The MGLO model is similar to the KMF one for $k \approx 1.5$–2. From the above-discussed list of models, only the SLO and KMF-T follow the strict form of the Brink hypothesis.

Next we tested two models available in the recent PSF review [4], which provide both $S^{(E1)}$ and $S^{(M1)}$: namely, the PSF model labeled as QRPA+D1M+0lim based on QRPA (quasiparticle random-phase approximation) calculations with the D1M Gogny interaction complemented with a phenomenological nonzero limit $S_{0\text{lim}}$ for $E_\gamma \to 0$, and the simplified modified Lorentzian (SMLO) model [51]. We also tested additional PSFs based on the QRPA calculations using several different forms of Skyrme effective interaction [52–54]; for a brief description of these PSFs see the Appendix. We also checked the impact of adding the same $S_{0\text{lim}}$ as used in [4] to these calculations.

The γ-ray energy dependence for several $S^{(E1)}$ models is shown in Fig. 5. Two curves for the MGLO and SMLO model illustrate their dependence on the nuclear temperature, the lower curve corresponds to $T = 0$ (transitions to the ground state) and the upper one represents primary transitions. PSFs from QRPA-based models with different interactions can then be found in Fig. 14.

2. Magnetic dipole PSF

Magnetic dipole ($M1$) transitions also play an important role in the γ decay of deformed rare-earth nuclei below S_n. The impact of $M1$ transitions is especially due to the presence of the scissors mode. The SM as a concentration of the ground-state $M1$ strength was envisaged from theory [6,7,55] and discovered in (e, e') measurements [56,57]. A wealth of information on the SM was gathered especially in nuclear resonance fluorescence (NRF) experiments [14,58], which determine the individual reduced transition probabilities $B^{(M1)}$. The manifestation of the SM in the decay of excited states (at least approximately obeying the Brink hypothesis) was then reported from TSC [47,59], MSC [8–10,48], and Oslo [11,46,60] experiments; the first two techniques confirmed the $M1$ character of the mode.

With the exception of the PSF given by the QRPA calculations [51–54] and the SMLO model [51], we described $S^{(M1)}$ with a composite model $S^{(M1)} = S^{(M1)}_{\text{SM}} + S^{(M1)}_{\text{SF}} + S^{(M1)}_{\text{SP}}$, with the first two terms representing the scissors and spin-flip (SF) modes of the Lorentzian shape, and the last term the possible single-particle (SP) contribution, a constant PSF. In our simulations, the SM was exclusively represented with a single-resonance term, and the SF with a double-peaked structure, based on the (p, p') data [61]. The composite model aims to describe a potentially complicated behavior of the $M1$ PSF.

In addition, a strong low-energy PSF enhancement—reported before from Oslo-type experiments only in lighter nuclei—was recently observed also in heavier nuclei, including rare-earth ones [62]. A possible influence of this phenomenon was tested as well. A strict validity of the Brink hypothesis was assumed for all adopted $S^{(M1)}$ models.

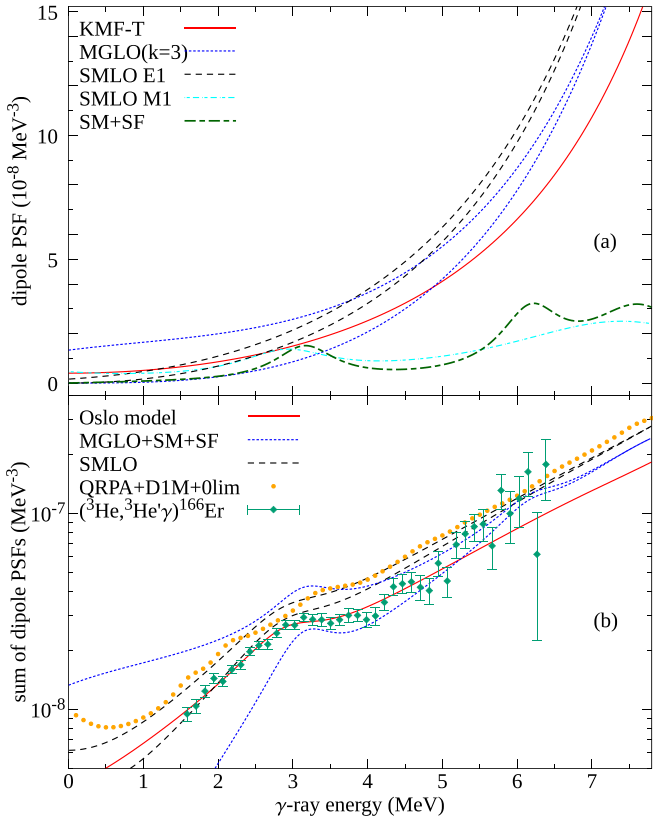

FIG. 5. Photon strength functions as a function of γ-ray energy for some of the models tested in our simulations. For the Oslo model (KMF-T) with $T = 0.31$ MeV the corresponding $M1$ parameters were taken from [12]. The parameters of SM+SF are $E_{\rm SM} = 3.2$ MeV, $\Gamma_{\rm SM} = 1.0$ MeV, $\sigma_{\rm SM} = 0.5$ mb and $E_{\rm SF,1} = 6.2$ MeV, $\Gamma_{\rm SF,1} = 1.0$ MeV, $\sigma_{\rm SF,1} = 1.7$ mb and $E_{\rm SF,2} = 7.7$ MeV, $\Gamma_{\rm SF,2} = 1.8$ MeV, $\sigma_{\rm SF,2} = 2.6$ mb. (a) Commonly used $E1$ and $M1$ models. The two curves for MGLO and SMLO models reflect the temperature dependence of the models, the lower curve corresponds to $T = 0$ and the upper one to $T = \sqrt{(S_n - E_\gamma - \Delta_P)/a}$. (b) The sum of $E1$ and $M1$ models from the upper panel. The experimental data on (^{3}He, ^{3}He$'$ γ) ^{166}Er are from Ref. [12].

D. Efficiencies needed for isomeric ratio

Experimental determination of $R_{\rm iso}$ in Eq. (1) requires the knowledge of three different efficiencies. All three were obtained from the GEANT4 simulations of detector response to individual simulated cascades using the above-specified conditions. The best models reproducing the MSC spectra to the ground state were adopted for calculation of $\varepsilon_{\rm pr}$ and $\varepsilon_{\rm feed}$. We verified that different models which acceptably describe the MSC spectra give very similar values of the required efficiencies. Note that the last efficiency, $\varepsilon_{\rm iso}$, is independent of the used model as it is given by the decay of the isomeric state adopted from literature [17].

IV. TESTS OF NLD AND PSF MODELS USING MSC SPECTRA

We compared the mean experimental MSC spectra with their simulated counterparts to draw conclusions about the predictions of different NLD and PSFs models. The results for the available model combinations from the literature are discussed in Sec. IV A, the spectra for PSFs based on QRPA calculations with Skyrme interaction are presented in Sec. IV B, and a search for the optimal combination of NLD and PSFs is then described in Sec. IV C.

As discussed in detail below, we are very sensitive to some of the SM properties, especially to its energy $E_{\rm SM}$. All PSF models that do not have the scissors mode energy in a narrow range of $E_{\rm SM} \approx 2.9$–3.3 MeV will not be able to provide satisfactory description of experimental spectra.

To correctly quantify the degree of agreement between the simulated and experimental MSC spectra, enormously time-consuming simulations with an extremely large number of NRs would be needed as the contents of individual bins in the MSC spectra are mutually correlated in a very complicated fashion and the corresponding correlation matrix is *a priori* not known. We tested a simple numerical goodness-of-fit scoring function, but such a criterion was found to be largely inconclusive. As a consequence, within the search for suitable PSFs and NLD models, the degree of agreement was checked visually. However, we stress that the high sensitivity of our experimental observables enables us to reject many models and significantly restrict the parameter space using this method.

The simulated spectra are plotted as a band, where the center corresponds to the average value over the set of 20 NSs. The width of the band is given by two standard deviations of the set (the average $\pm 1\sigma$). Only spectra for $M = 2$–4 are shown below as there are no visible structures for $E_\gamma \gtrsim 1$ MeV (as indicated for $M = 5$ in Fig. 3).

A. Model combinations from literature

Predictions of the two models proposed in the recent PSF review [4], the QRPA+D1M+0lim and the SMLO, are compared to the average experimental spectra in Fig. 6; the NLD model, indicated in the figure caption, gives the best reproduction of experiment. Although the overall description of the spectra might look reasonable, the agreement is far from perfect. Specifically, the QRPA+D1M+0lim model has a problem with the reproduction of $E_\gamma \approx 2$–4 MeV for $M = 3$ and 4. This is a consequence of the properties of the $S^{(M1)}$ in the SM region, in particular the aforementioned misalignment of $E_{\rm SM}$. The SMLO model predictions yield a different type of inconsistency: while the SM region in $M = 3$ and 4 is described better, the predicted MSC intensities in the center of $M = 2$ spectra are considerably larger than the experimental ones.

Although there are no experimental data from the Oslo method for ^{168}Er, they exist for the neighbor even-even nucleus ^{166}Er. Similar deformation of the two nuclei should lead to very similar PSFs in them. We thus decided to test the PSFs proposed for ^{166}Er in Ref. [12], given by the KMF-T $E1$ and SM+SF $M1$ contributions (we assumed the $M1$ origin of "pygmy resonance" near 3 MeV). The use of experimental NLD from the Oslo measurement [12] is problematic, as the one proposed for ^{166}Er does not reproduce the resonance spacing in the ^{168}Er compound nucleus, the Oslo NLD seems

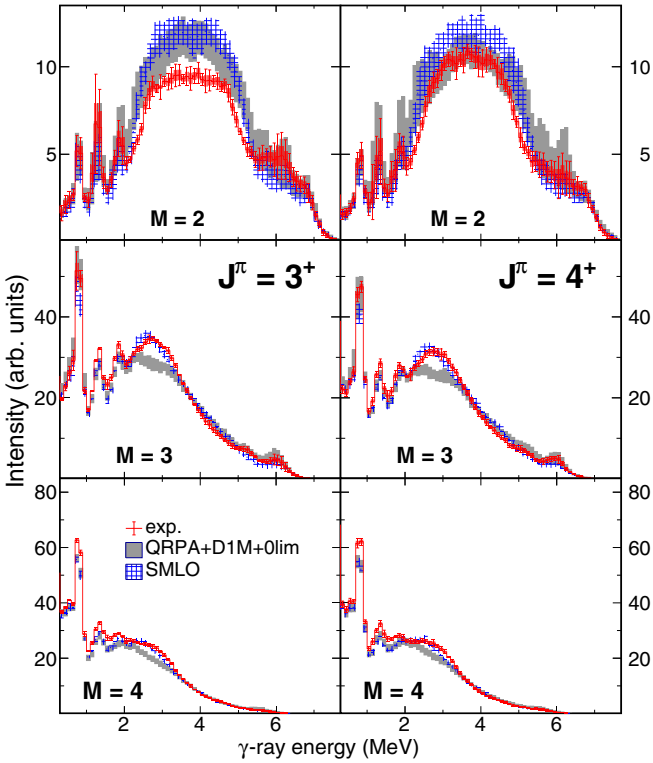

FIG. 6. Mean experimental MSC spectra for $J^\pi = 3^+$ (left) and 4^+ (right) neutron resonances and multiplicities $M = 2-4$ compared to the simulated MSC spectra using the QRPA+D1M+0lim [51] (gray) and the SMLO [51] (blue) PSF models. The HFB calculated NLD [41] was used for the QRPA+D1M+0lim, and the BSFG NLD model [37] was used for the SMLO. The mean experimental intensities and their uncertainties are shown as full red rectangles. The red error bars correspond to the fluctuation of the intensities. The simulated MSC spectra are drawn as gray and blue bands corresponding to a two-standard-deviation corridor centered at the average.

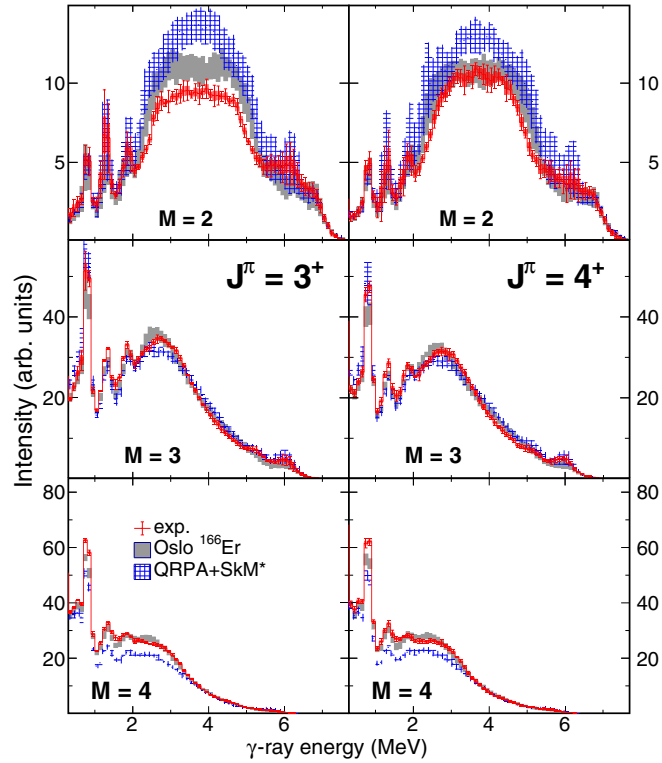

FIG. 7. Mean experimental MSC spectra for $J^\pi = 3^+$ (left) and 4^+ (right) neutron resonances and multiplicities $M = 2$–4 compared to the simulated MSC spectra using the Oslo [12] (gray) and QRPA + SkM* (blue) PSF models. The HFB calculated NLD [41] was used for the QRPA + SkM*, and the BSFG NLD model [37] was used for the Oslo model. The meaning of the symbols is analogous to the Fig. 6.

to be consistent with BSFG model therein. The predicted MSC spectra in combination with the BSFG NLD can be found in Fig. 7. The reproduction of the experimental spectra with Oslo-based PSFs is better than with the models from review [4]; the only clear disagreement is visible in $M = 2$ spectra: the most pronounced difference is the overestimation of intensities from $J = 3$ resonances for $E_\gamma \approx 2.5$–5 MeV.

B. PSFs based on QRPA with Skyrme interaction

In addition to the QRPA+D1M+0lim we simulated MSC spectra also for PSFs based on QRPA calculations with several Skyrme effective interaction parametrizations described in the Appendix; see Fig. 7 and additional figures in [31]. We decided to check these PSFs in three different ways: (i) by adopting the exact results of the calculations, (ii) by shifting the calculated $M1$ strengths by Δ_E in a way that the strongest predicted bump below 5 MeV has its centroid at $E_\gamma \approx 3.2$ MeV, and (iii) by adding the empirical $S_{0\mathrm{lim}}$ to the calculated PSFs.

As is evident from Fig. 14 in the Appendix only the SkM* interaction predicts the position of the SM in the aforementioned required range just above 3 MeV. We verified that only this parametrization can acceptably reproduce the SM region in $M = 3$ spectra; all others significantly underestimate the intensity there. Application of Δ_E improves the agreement with the experiment near 3 MeV in $M = 3$ spectra but we have never reached a simultaneous reproduction of MSC spectra for all M with any used parametrization; the best reached agreement is shown in Fig. 7. Predictions are very similar with both the HFB and BSFG NLD models.

Adding $S_{0\mathrm{lim}}$ typically leads to an improvement by reduction of the predicted intensity in the center of $M = 2$ MSC spectra, but it leads to the reduction of the intensity around $E_\gamma \approx 3$ MeV in $M = 3$ MSC spectra that worsens the agreement. The problem with reproduction of the peak near 3 MeV in $M = 3$ MSC spectra, observed for the majority of parametrizations without $S_{0\mathrm{lim}}$ and for all of them with $S_{0\mathrm{lim}}$, results from a relative deficit of SM strength around 3 MeV. Note that the two parametrizations that are able to reproduce the 3-MeV peak in $M = 3$ MSC spectra without $S_{0\mathrm{lim}}$, SkM*, and Vba do not show any peak near 2 MeV in $S^{(M1)}$; this lower-energy peak from the other parametrizations

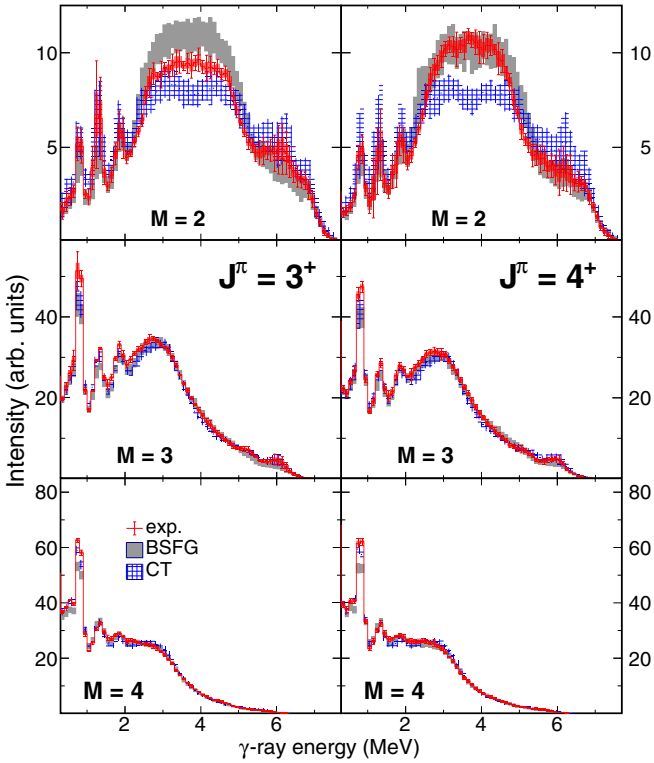

FIG. 8. Mean experimental MSC spectra for $J^\pi = 3^+$ (left) and 4^+ (right) neutron resonances and multiplicities $M = 2$–4 compared to the simulated MSC spectra using the BSFG NLD model [37] (gray) and CT NLD model [37] (blue). The MGLO($k = 3$) $S^{(E1)}$ model and the composite $S^{(M1)}$ model with the adjusted SM parameters were used in the simulations. The meaning of the symbols is analogous to Fig. 6.

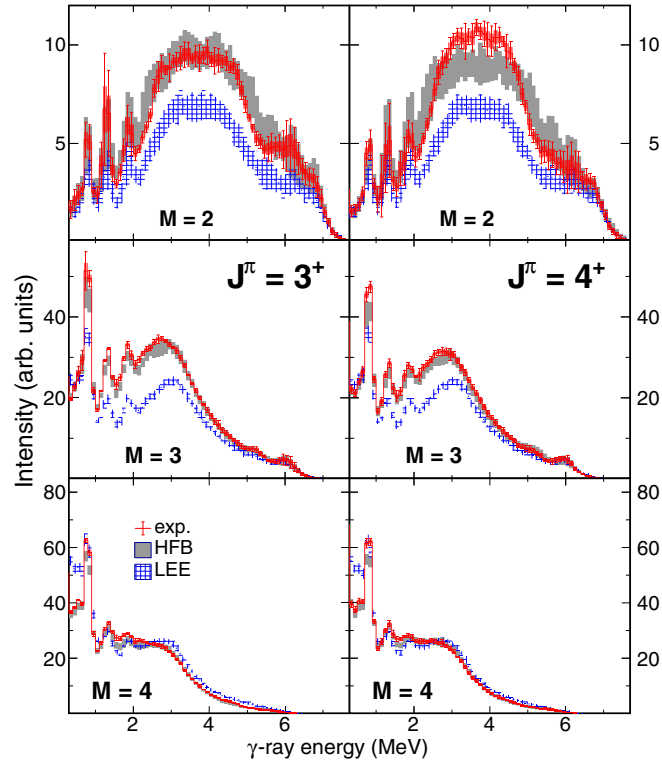

FIG. 9. Mean experimental MSC spectra for $J^\pi = 3^+$ (left) and 4^+ (right) neutron resonances and multiplicities $M = 2$–4 compared to the simulated MSC spectra using the HFB NLD model [41] (gray) and the BSFG NLD model [37] with LEE contribution [62] to $S^{(M1)}$ (blue). The MGLO($k = 3$) model for $S^{(E1)}$ and a composite model for $S^{(M1)}$ with the SM parameters $E_{\rm SM} = 3.2$ MeV, $\Gamma_{\rm SM} = 1.0$ MeV, and $\sigma_{\rm SM} = 0.6$ mb and zero $S_{\rm SP}$ were used; see also Fig. 5. The meaning of the symbols is analogous to Fig. 6.

surely reduces the 3-MeV peak strength in $S^{(M1)}$. The same happens if $S_{0\rm lim}$ is considered.

C. Search for optimal PSFs and NLD

The above-tested models do not perfectly reproduce experimental MSC spectra: there are problems especially with reproducing the $M = 2$ central region and the exact position of the $E_\gamma \approx 3$ MeV structure in $M \geqslant 3$. We thus performed a search to obtain a better description via sampling of the $S_{\rm SP}^{(M1)}$ and $S_{\rm SM}^{(M1)}$ parameters in combinations with several different $S^{(E1)}$ and NLD models. The results from this search related to individual involved quantities are presented below. Similarly to the aforementioned comparisons, we typically have a problem with simultaneous reproduction of spectra from both resonance spins and, especially for spectra from $J = 3$ resonances, with reproduction of the central part of $M = 2$ and $E_\gamma \approx 2$–3 MeV region in $M = 3$.

1. Level density

The experimental MSC spectra cannot be reproduced with the CT model for any tested combination of PSF models. A very different SM strength was required to describe $M = 2$ and $M > 2$ spectra with this NLD model. Figure 8 illustrates the case where the strong postulated SM leads to a good agreement for the latter spectra but completely fails in the reproduction of $M = 2$. On the other hand, the BSFG and the HFB models yielded a much better agreement. The best overall reproduction was reached with the model based on HFB calculations [41], which is shown in Fig. 9; predicted spectra with the BSFG model are very similar (see Fig. 8). The only deviation for the HFB model from the experimental shape was observed in $M = 2$ spectra for spin $J = 4$, where the central part of $E_\gamma \approx 3$–5 MeV is underestimated in the simulations. The BSFG model then slightly overestimates experimental intensities for $M > 4$ spectra. The results with the BSFG model were virtually independent of the adopted parametrizations [36,37] and of the checked even-odd staggering and parity dependence [38] described in Sec. III B.

2. E1 PSF

We were unable to reproduce the MSC spectra with any model combination including SLO $S^{(E1)}$, as we cannot match the experimental multiplicity distribution; in particular, it significantly overestimates the central part of $M = 2$ spectra. Further, the predictions with the EGLO $S^{(E1)}$ model yield a too

strong contribution of higher M compared to the experiment as a result of a large $S^{(E1)}$ at low E_γ.

A reasonable reproduction was achieved only with the KMF, KMF-T ($T = 0.3$–0.35 MeV), and MGLO($k = 2$–3) models. Probably the best overall agreement is given by the MGLO($k = 3$) $S^{(E1)}$; see Figs. 8 and 9. The acceptable models indicate that we cannot confirm or reject the strict validity of the Brink hypothesis.

3. M1 PSF

The reproduction of bumps near 2.5 MeV in $M = 3$ and 4 MSC spectra requires a resonance structure in $S^{(M1)}$ near 3 MeV; tests with a resonance in $S^{(E1)}$ never worked. Satisfactory reproduction was provided by $E_{\rm SM} = 3.1$–3.3 MeV and $\Gamma_{\rm SM} = 0.8$–1.3 MeV almost independently of the employed $E1$ PSF model. Especially the sensitivity to the resonance position is remarkable.

As our simulations are mainly sensitive to the relative E_γ dependence of the PSFs, the allowed SM strength (given usually by the maximum cross section $\sigma_{\rm SM}$) scales with the absolute value of $S^{(E1)}$. The allowed $\sigma_{\rm SM}$ in combination with the MGLO($k = 3$) in the parametrization from Dietrich and Berman [42] is $\sigma_{\rm SM} = 0.4$–0.6 mb. For further discussion of the SM strength see Sec. V B. The SP part of the composite $S^{(M1)}$ must be very weak, $S^{(M1)}_{\rm SP} \lesssim 2 \times 10^{-9}$ MeV^{-3}. A larger $S^{(M1)}_{\rm SP}$ shifts the multiplicity distribution towards too high values.

In order to examine the possibility of a low-energy enhancement (LEE) of $S^{(M1)}$, we adopted the LEE part of $S^{(M1)}$ in the same form as proposed by Simon *et al.* [62]. We were not able to reproduce the experimental MSC spectra, as the LEE introduces a large amount of low-E_γ transitions that result in lack of intensity for low M; see Fig. 9. The LEE part of $S^{(M1)}$ was also proposed in Ref. [4], albeit more than two orders of magnitude weaker. Our data are insensitive to such low LEE.

D. Fluctuations of MSC spectra

In the statistical model, strong fluctuations of individual decay intensities are assumed for levels above $E_{\rm crit}$; they are governed by the PT distribution. Within our approach, this assumption can be tested by comparing the experimental and simulated fluctuations of the MSC spectra. Such a fluctuation analysis has already been performed for two even-even Dy isotopes [10] and ^{196}Pt [30].

The number of observed resonances allowed us to perform a similar analysis also for the decay of ^{168}Er. For this purpose we have run extended simulations with 50 NRs within each of 50 NSs for the model reasonably describing MSC spectra to the ground state, shown in Fig. 10. From these simulations we determine for the MSC intensity its mean value, μ, the average expected fluctuations over different NRs within a NS, ϕ, and total fluctuations from all NRs and NSs, ϕ_T. These quantities are shown in Fig. 10.

In accord with the Dy and Pt results, the analysis indicates that the fluctuations among different NRs within a fixed NS, ϕ, are dominant and the fluctuations of averages from different NSs are much smaller. This feature justifies the above-applied use of only one NR from several different NSs for testing the adequacy of different PSFs and NLD models.

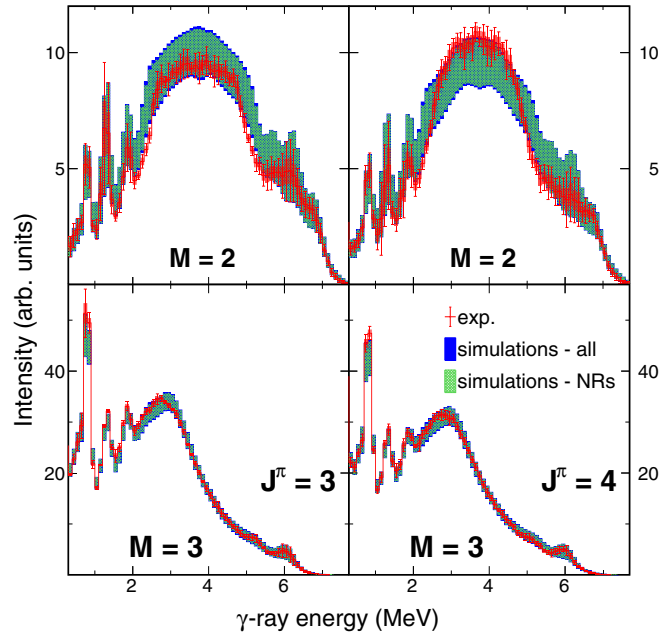

FIG. 10. Comparison of MSC intensities and their fluctuations from experiment and extended simulations for both resonance spins $J^\pi = 3^+$ (left) and $J^\pi = 4^+$ (right) and $M = 2$–3. The model combination labeled HFB in Fig. 9 was used. The experiment is plotted as in Fig. 6: the green band corresponds to average fluctuations over NRs ($\mu \pm \phi$) and the blue band indicates the total fluctuations ($\mu \pm \phi_T$); for details see Sec. IV D.

Assuming that the fluctuations are correctly described in our simulations, we should not only require agreement between the mean experimental and simulated MSC intensity but also the estimate of ϕ should be comparable to $\phi_{\rm exp}$. From Fig. 10 it is clear that $\phi_{\rm exp} < \phi$ for the majority of the bins, with a typical ratio of about 2, similar to our results in Dy and Pt.

Although the difference in fluctuations might indicate their inadequate treatment in the simulations, we have a couple of comments on the results. First, the tested model combination does not reproduce experimental spectra perfectly. It is expected that simulated fluctuations do depend on the adopted combination of PSFs and especially NLD models; a different number of simulated levels in the excitation energy interval corresponding to the E_γ range can significantly change the simulated fluctuations. Note that even in $M = 2$ MSC spectra, E_γ does not directly correspond to the excitation energy. Furthermore, while the assumptions used in the DICEBOX code seem to be well justified for highly excited states such as neutron resonances, there might be additional nonstatistical effects in the decay of levels at energies just above $E_{\rm crit}$, which might also be responsible for our inability to perfectly reproduce the MSC spectra. As a result, it seems rather difficult to make any definite conclusions about the validity of the PT fluctuations of individual transition intensities in ^{168}Er. Nevertheless, the similarity of results in all tested cases points

TABLE I. Total radiative width of s-wave resonances $\overline{\Gamma}_\gamma$ based on the GEDR parametrization from ^{nat}Er [42]. The parametrizations from [37] were used for the BSFG and CT NLD; $\overline{\Gamma}_\gamma$ with parametrizations from [36] are very similar, they differ at most by 3%. Note that rescaling of $S^{(E1)}$ by a constant factor implies the same rescaling of $S^{(M1)}$, and hence also of $\overline{\Gamma}_\gamma$.

Model		$\overline{\Gamma}_\gamma$
PSF	NLD	(meV)
QRPA+D1M+0lim [4]	HFB	121(3)/82(2)[a]
SMLO [4]	BSFG	115(2)
Oslo [12]	BSFG	86(3)
MGLO($k=3$)	HFB	138(3)/93(2)[a]
MGLO($k=3$)	CT	56(1)
MGLO($k=3$)	BSFG	125(3)
MGLO($k=3$) rescaled	BSFG	91(2)
MGLO($k=2$)	BSFG	102(2)
Compilation [27]		91.0(16)

[a]Two values correspond to $\overline{\Gamma}_\gamma$ for resonances with spin 3 and 4, respectively.

out a common issue in the current use of the statistical model, which needs to be further investigated.

V. COMPARISON WITH OTHER DATA

The proposed PSF and NLD models are similar to those reproducing the MSC spectra in several well-deformed even-even rare-earth nuclei [8–10] with different neutron separation energies and from resonances of different spins and parities. We thus have a high confidence that the used trial-and-error approach yields models that are very close to reality.

A. Total radiative width of neutron resonances

The total radiative width Γ_γ is the only detector-independent quantity simulated in DICEBOX that depends on the absolute values of PSFs. Experimentally observed differences in the individual Γ_γ from resonance shape analysis of neutron resonances are caused by fluctuations of intensities of primary transitions and reach at most a few percent of the average value $\overline{\Gamma}_\gamma$. The calculated values of $\overline{\Gamma}_\gamma$ for several model combinations are listed in Table I together with value from Mughabghab's compilation [27].

Γ_γ is given by a sum of contributions from each type and multipolarity; in DICEBOX it is approximated by $\Gamma_\gamma = \Gamma_\gamma^{(E1)} + \Gamma_\gamma^{(M1)} + \Gamma_\gamma^{(E2)}$. It turns out that the dominant contribution comes from $E1$ transitions. The contribution of the scissors mode is about 15%. The combined contribution of SF and the $E2$ transitions reaches at most ≈5%.

As can be seen in Table I, the value of $\overline{\Gamma}_\gamma$ further significantly depends on the adopted NLD model. This is due to the number of levels available for primary transitions, and the resonance spacing D_0. In practice, the NLD models are typically fixed to experimental D_0, hence there is effectively no dependence on D_0. For a given set of PSF models, the BSFG NLD gives about two times higher $\overline{\Gamma}_\gamma$ than the CT one (independently of the checked NLD parametrization). For these two NLD models the difference in $\overline{\Gamma}_\gamma$ between two s-wave resonance spins is smaller than 3%. The HFB model then yields very different $\overline{\Gamma}_\gamma$ for resonances of each spin: for $J=3$ ones $\overline{\Gamma}_\gamma$ is higher by about 10% than the BSFG NLD prediction, while for $J=4$ it gives about 75% of this value. This difference, presented in Table I, comes from the very different spin behavior of the HFB model, which shows significant even-odd spin staggering even at S_n, and is in very strong disagreement with compiled data [27].

As mentioned in Sec. III C, there are two available GEDR parametrizations, which significantly differ in the absolute PSF values below S_n, they thus lead to very different $\overline{\Gamma}_\gamma$. The RIPL-3 parametrization [5,43] yields a simulated $\overline{\Gamma}_\gamma^{(E1)}$ larger by about a factor of 1.35 than the one from Dietrich and Berman [42]. Their parametrization for ^{nat}Er is much closer to the ^{160}Gd one [42], which was used in the studies of the MSC spectra for well-deformed Gd and Dy isotopes. The RIPL-3 parametrization [5,43] is inconsistent with the original work [63] and the expectation that the GEDR parameters change slowly in nuclei of similar mass and deformation, which indicates that the RIPL-3 parametrization should be revisited. As a result, the $\overline{\Gamma}_\gamma$ values presented in Table I are calculated with the ^{nat}Er GEDR parametrization from Dietrich and Berman [42].

The model combinations, including MGLO($k=3$) $S^{(E1)}$, best describing the MSC spectra (see Figs. 8–10), overestimate $\overline{\Gamma}_\gamma$. This indicates that actual absolute scale of PSFs below S_n is not appropriate and/or that the actual NLD model behaves differently, perhaps in a more complicated fashion than given by traditionally used models. As mentioned above, the MSC spectra are not sensitive to the absolute values of PSFs if their energy-dependent ratios are kept the same. Hence, *ad hoc* rescaling of the MGLO($k=3$) $S^{(E1)}$ and corresponding $S^{(M1)}$ below S_n by a factor 0.728 can provide perfect agreement of $\overline{\Gamma}_\gamma$; see Table I.

B. SM strength

The scissors mode strength can be compared to those from the NRF and Oslo-type experiments. It is calculated from $S^{(M1)}$, which best reproduces the MSC spectra. For this comparison we adopted the $S^{(M1)}$ deduced in conjunction with MGLO($k=3$) $S^{(E1)}$ using the ^{nat}Er GEDR parametrization from Dietrich and Berman [42]. The absolute scale of both PSFs and hence strength of the SM are at question because of the inability to reproduce $\overline{\Gamma}_\gamma$; see our comments in Sec. V A. As a result, we present the SM strength with and without the above-mentioned *ad hoc* rescaling of the PSFs.

To compare our strength to the NRF ones, we calculated the total $M1$ contribution $\sum B^{(M1)}$ as an integral of $S^{(M1)}$ in the energy region $E_\gamma = 2.7$–3.7 MeV. The comparison of the strength for well-deformed Gd, Dy, and Er even-even isotopes is given in Fig. 11. Our deduced values $\sum B^{(M1)} = 3.23(88)\mu_N^2$ and $2.33(63)\mu_N^2$ with and without rescaling, respectively, follow the trend observed in the NRF analyses [14,58]. Note that the SM contributes to our derived $M1$ strength by ≈90%.

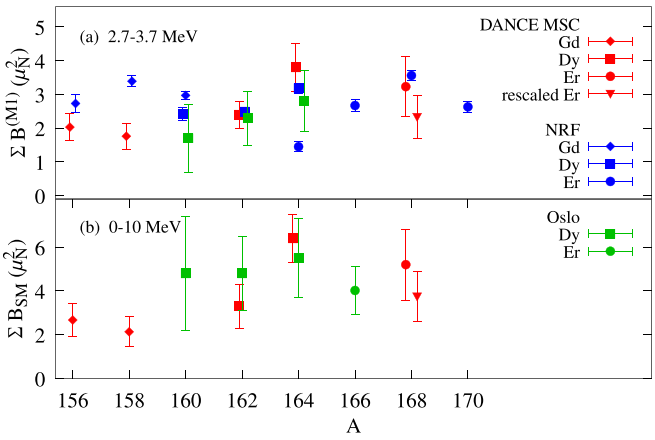

FIG. 11. Upper panel: Comparison of the total $M1$ strength in the 2.7–3.7 MeV range, $\sum B^{(M1)}$, for even-even isotopes of Gd, Dy, and Er as a function of mass number A. Lower panel: Comparison of the total SM strength $\sum B_{\mathrm{SM}}$ integrated for $E_\gamma = 0$–10 MeV. Our values from analysis of the MSC spectra for ^{168}Er are plotted together with analogous Gd [8,9] and Dy [10] results, data from (γ, γ') measurements [14,58], and Oslo method results for ^{166}Er [12] and Dy [64].

Furthermore, we determined the total SM strength $\sum B_{\mathrm{SM}}$ as an integral of S_{SM} over the range 0–10 MeV and compared it to the results from Oslo experiments for the Dy and Er even-even isotopes; see Fig. 11. The only Oslo result for Er is available for ^{166}Er. Our values, $\sum B_{\mathrm{SM}} = 5.20(162)\mu_{\mathrm{N}}^2$ and $3.74(116)\mu_{\mathrm{N}}^2$ with and without rescaling, respectively, are consistent with the value obtained for ^{166}Er [12].

VI. ISOMERIC RATIO

A. Experimental isomeric ratio

Determination of the R_{iso} required resonances with sufficient statistics and that are well separated in time of flight to avoid the contribution of the decay from the neighboring ones. We determined the R_{iso} only for a fraction of the resonances used in the analysis of the MSC spectra. In addition, we were also able to obtain R_{iso} for neutron energies $E_n = 0.2$–0.25 eV. This range, with a contribution from both resonance spins (about 23% of $J^\pi = 3^+$ based on [27]), offered very high statistics and was used for the check of the method as it allowed rather precise determination of the isomeric half-life. The experimental values of the R_{iso} obtained from Eq. (1) together with the deduced half-lives for individual resonances are presented in Table II. The given uncertainties come only from the uncertainty of the fit. All but one values of half-life are 2σ compatible with the literature value $T_{1/2} = 109.0(7)$ ns coming from the ENSDF evaluation of ^{168}Tm ε decay [17].

The efficiencies needed for the determination of R_{iso} [see Eq. (1)] were estimated using the model combination labeled HFB in Fig. 9; see also Fig. 5. The combined relative uncertainty from all efficiencies is below 2%. All models that reasonably reproduced the MSC spectra yielded efficiencies consistent within this uncertainty.

TABLE II. The experimental results on the isomeric ratio. The uncertainties are only from the fit.

J^π	E_{res} (eV)	$T_{1/2}$ (ns)	R_{iso} (%)
3^+	22.02	112.4(28)	17.3(5)
	39.43	103.0(31)	13.8(6)
	42.23	107.4(41)	15.2(11)
	59.96	109.8(46)	13.9(12)
	85.42	106.9(118)	15.3(22)
	107.6	109.8(28)	11.9(4)
4^+	50.19	105.8(34)	20.6(10)
	69.43	117.4(46)	27.1(13)
	91.20	119.1(61)	24.4(17)
	184.7	123.1(61)	26.9(21)
	217.2	121.4(76)	28.3(29)
	0.2–0.25	109.2(18)	23.6(3)

As the individual values are expected to fluctuate, we determined the mean value and the width of the distribution considering experimental uncertainties (similarly to the construction of the mean experimental MSC spectra). The mean R_{iso} are 14.5(8)% and 25.0(14)% and the widths of the distribution $\sigma_{R_{\mathrm{iso}}} = 1.7(6)$% and 2.5(10)% for $J^\pi = 3^+$ and 4^+ resonances, respectively. Using these mean values we expect the population about 22.6(11)% in the $E_n = 0.2$–0.25 eV, consistent with the experimental value of 23.6(3)%. The R_{iso} determined from intensities of depopulating transitions reported in the ENSDF $(n_{\mathrm{th}}, \gamma)$ evaluation is 26.6(10)% [17]; our mean values yield 21.4(10)% considering the contributions of each resonance spin to the thermal energy from [27]. We have two comments on this. First, the ENSDF gives intensities of the isomeric decay as the average from two measurements [65,66]; the newer one reports intensities systematically smaller by about 5–10% than the ENSDF average. The use of the intensities from Ref. [66] would thus slightly reduce the reported depopulation in the thermal capture. Second, the isomeric ratio from individual resonances shows fluctuations, and their estimate $\sigma_{R_{\mathrm{iso}}}$ indicates that they are rather large. The contributions of first three resonances dominate the R_{iso} values both at thermal energy and in the $E_n = 0.2$–0.25 eV interval (with different contributions). The $R_{\mathrm{iso}} = 23.6\%$ in the $E_n = 0.2$–0.25 eV interval implies that R_{iso} for 0.46 eV resonance is $\lesssim$25%. This value makes it impossible to reach $R_{\mathrm{iso}} \approx 26\%$ at thermal energy, because the 0.46 eV resonance dominates with 2/3 contribution at thermal energy and all $J = 3$ resonances have lower R_{iso}. We have not found any solid explanation for this inconsistency.

B. Simulated isomeric ratio

Experimental R_{iso} can be compared to the values obtained from the DICEBOX predictions. Rich information on the levels of ^{168}Er at low excitation energy allowed us to check the impact of the possible "nonstatistical" effects on R_{iso} present in the decay of levels up to about 2.4 MeV. Such a check was performed using a series of simulations with different E_{crit}; the results are presented in Fig. 12.

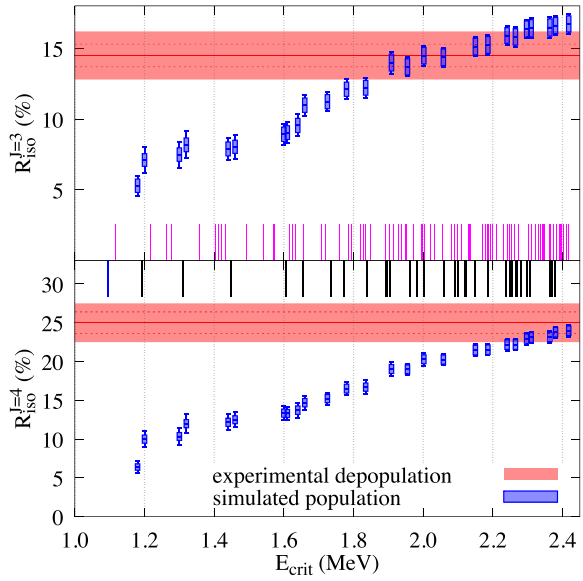

FIG. 12. Predicted R_{iso} as a function of the critical energy for capturing state spins $J = 3$ (upper panel) and 4 (lower panel) using the model combination labeled HFB in Fig. 9; see also Fig. 5. For simulations the fill corresponds to the width of the distribution of values from individual NRs, while the error bar shows the overall fluctuation over all NSs and NRs. The average experimental value with its uncertainty is indicated by full and dashed lines, respectively. The width of the distribution is shown as a red band. The excitation energies of the isomer, isomer-feeding levels, and other levels are marked by the blue, black, and magenta lines, respectively.

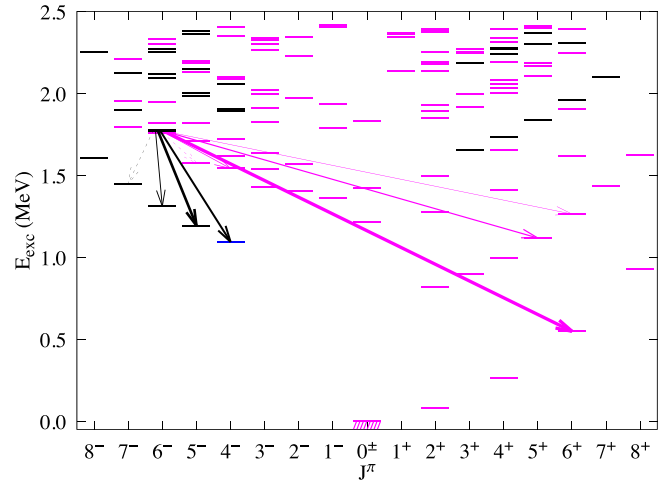

FIG. 13. Schematic representation of ^{168}Er low-lying level scheme with the decay of the $J^{\pi} = 6^-$ level at 1760.8 keV (magenta arrows) and the 6^- isomer-feeding level at 1773.2 keV (black arrows). The isomer is drawn in blue, isomer-feeding levels in black, and the other levels in magenta.

The predicted R_{iso} is significantly lower than the actual one if we completely neglect any "structural" effects above the isomer (considering the lowest checked E_{crit}). The observed increase of the simulated R_{iso} is then caused by the presence of levels dominantly decaying to the isomer. Let us denote such a level, which feeds not necessarily directly the isomer, as an *isomer-feeding level*. In the case of ^{168}Er the distinction of the low-lying levels is often clear, e.g., the $J^{\pi} = 6^-$ level at 1760.8 keV decays (both directly and indirectly) mostly to the two lowest-lying positive-parity rotational bands and is definitely not an isomer-feeding level. On the other hand, the 6^- level at a very similar energy of 1773.2 keV decays exclusively to the isomeric rotational band and is without any doubt an isomer-feeding level; see Fig. 13. For more complicated cases we have used an arbitrary criterion: if at least 80% of the branching intensity feeds, not necessarily directly, the isomer, the level is considered an isomer-feeding one. Based on information from [17], there are 21 isomer-feeding levels below 2.2 MeV, and 32 below 2.42 MeV.

Including an isomer-feeding level of suitable spin at low energy can increase R_{iso} by a few percent; see Fig. 12. On the other hand, the population of a single level (within the statistical model) near our highest E_{crit} does not exceed 0.4% and it exponentially decreases (halves in about 300 keV). Therefore a single isomer-feeding level at higher excitation energy does not induce such a strong effect, yet the abundance of these levels does result in increasing R_{iso}, clearly visible from Fig. 12 at least for 4^+ resonances up to the highest adopted E_{crit}; no significant increase in R_{iso} is visible for 3^+ resonances above $E_{crit} \approx 2.3$ MeV. This feature means that the statistical description of γ decay is not fully adequate for levels at least up to excitation energies close to the highest checked E_{crit}. Higher values of E_{crit} could not be tested as the evaluated level scheme [17] starts to suffer from missing levels (see Fig. 4) and missing information on level properties.

Such a result is in accord with the presence of structures in $M = 2$–4 MSC spectra that cannot be described with E_{crit} lower than about 2.3–2.4 MeV. The absence of any narrow structure in MSC spectra above $E_{\gamma} \approx 2$ MeV could then indicate that nonstatistical effects are much weaker at higher excitation energies.

The dependence of R_{iso} on E_{crit} is very similar for all models that acceptably reproduce MSC spectra although there are some differences in the R_{iso} absolute value. The predicted R_{iso} with the BSFG NLD model are by about 10% smaller (for all E_{crit}) than those with the HFB model. As a consequence, we have a problem with the exact simultaneous reproduction of the isomeric ratio for both resonance spins: the predicted R_{iso} with the highest E_{crit} is either already above the experimental average for 3^+ resonances (as shown in Fig. 12) or below the experimental average for 4^+ resonances; the deviations are on the level of two to three standard deviations for the worse case.

VII. SUMMARY

The coincident measurement of γ rays from the radiative neutron capture on ^{167}Er was performed with the DANCE detector array at the LANSCE spallation neutron source. Detected γ rays were used for the construction of the multistep γ ray spectra for different multiplicities and for checking the population of the 1094-keV $T_{1/2} = 109$ ns isomeric state in ^{168}Er.

The MSC spectra were used to test the validity of various PSF and NLD models via comparison of the simulated and

experimental spectra. Although we were unable to find a combination of models that would perfectly reproduce experimental spectra, we can make the following restrictions.

The MSC spectra are reasonably described using the BSFG [36,37] or the HFB [5,40,41] nuclear level density models. The spin dependence of the HFB model is unrealistic, as the predicted total radiative width of s-wave neutron resonances significantly depends on their spin, which is at variance with the available experimental data. The MSC spectra are virtually insensitive to a possible parity dependence and staggering between odd and even spins at low excitation energies.

A resonance-like structure in the $M1$ PSF with its centroid between 3.1 and 3.3 MeV and a width of about 1 MeV, which can be identified with the scissors mode, was found essential for the description of the MSC spectra. The SM strength is likely comparable to that from neighboring even-even well-deformed nuclei. The KMF- or MGLO-like models well describe the $E1$ PSF; it likely reaches a nonzero low-energy limit. These PSFs are nicely consistent with the ones of even-even Gd [8,9] and Dy [10] isotopes. On the other hand, the PSF shape featuring a strong low-energy enhancement [62] can be definitely ruled out.

A very reasonable reproduction of the experimental MSC spectra was achieved with the PSF for ^{166}Er from the Oslo-type experiment; such an agreement between these two methods is not usual even in well-deformed nuclei; see for example the case of ^{162}Dy [10]. We also checked different PSF models based on the QRPA calculations with Gogny D1M as well as a few Skyrme interaction parametrizations. Cascades generated with these models did not reproduce the measured MSC spectra.

The number of resonances allowed us to analyze the fluctuations of the MSC intensities. Similarly to the results from the previous analyses of ^{162,164}Dy and ^{196}Pt, the observed fluctuations among different neutron resonances of a given spin are significantly smaller than the predicted ones for broad ranges of γ-ray energies and multiplicities. This observation may indicate the invalidity of the assumed Porter-Thomas distribution of the primary transition intensities. Nevertheless, the situation is more complicated due to the assumptions imposed in the statistical model simulations, e.g., that all levels above $E_{\rm crit}$ decay statistically. In any case, further investigation of this phenomenon is really necessary.

The presence of the narrow structures in the $M = 2$ MSC spectra indicates that the statistical description of γ decay is not fully adequate for levels below at least 2 MeV. This behavior is confirmed by the analysis of the population of the isomeric state that showed the presence of nonstatistical effects up to even higher energy. Nonetheless, an overall reasonable reproduction of the experimental MSC intensities for both spins of the capturing states indicates that the widely used description of γ decay within the statistical model and the concept of PSFs is at least a very good approximation at energies above about 2–2.4 MeV for deformed even-even rare-earth nuclei.

In contrast to the previous analyses of the isomeric population of rare-earth nuclei (Hf [18], Lu [20]) from neutron capture, our simulated $R_{\rm iso}$ is compatible with the experimentally determined one in ^{168}Er if sufficiently high $E_{\rm crit} \approx$ 2.4 MeV is used. To our knowledge, this is the first time the reproduction of the $R_{\rm iso}$ in rare-earth nuclei was achieved. The reproduction was possible only due to extremely rich information on levels at low excitation energies in this nucleus, which is available up to an energy well above 2 MeV. If the nonstatistical effects play a role up to similar energies in other rare-earth nuclei, the reproduction of $R_{\rm iso}$ based on statistical decay models should not be expected.

ACKNOWLEDGMENTS

S.V. would like to express his thanks to O. Roig for his hospitality during the visit at CEA Bruyères Le Châtel and for his explanation of their analysis. The authors thank R. Casten for helpful comments as well as for the Er sample. This work was supported by U.S. Department of Energy Grants No. DE-NA0001784 and No. DE-FG02-97-ER41042, by Grant No. 23-06439S of the Czech Science Foundation, and by the Charles University projects UNCE/SCI/013, SVV 260576, and GAUK 590218. This work benefited from the use of the LANSCE accelerator and was performed under the auspices of the U.S. Department of Energy at Los Alamos National Laboratory by TRIAD National Security, LLC under Contract 89233218CNA000001. The ^{167}Er sample used in this research was supplied by the U.S. Department of Energy Isotope Program, managed by the Office of Isotope R&D and Production.

APPENDIX: PSFS FROM QRPA WITH THE SKYRME EFFECTIVE INTERACTION

The excitation QRPA PSF, $S^{(XL)}$, is given by (see, e.g. [67])

$$S^{(XL)}_{\rm gr\to J^\pi}(E_\gamma,\Gamma) = \sum_{K=-L}^{+L}\sum_i B_{ex}(XL;\ {\rm gr}\to iE_iK\pi)\,\frac{1}{2\pi} \times \frac{\Gamma}{(E_\gamma-E_i)^2+\Gamma^2/4} \xrightarrow{\Gamma\to 0} \sum_{K=-L}^{+L} B_{ex} \times (XL;\ {\rm gr}\to iE_iK\pi)\ \delta(E_\gamma-E_i), \quad \text{(A1)}$$

where

$$B_{ex}(XL;\ {\rm gr}\to iE_iK\pi) = \left|\langle iE_iK\pi|\hat{M}^{(XL)}_K|{\rm gr}\rangle\right|^2 \quad \text{(A2)}$$

is the reduced excitation probability of the XL transition from the RPA ground state $|{\rm gr}\rangle$ of the intrinsic Hamiltonian into the RPA one-phonon state $|iE_iK\pi\rangle = \hat{Q}^+_{i\pi K}\,|{\rm gr}\rangle$ with the excitation energy E_i, angular momentum projection K, and parity π (index i enumerates individual solutions of the QRPA equation for given K and π). The symbol $\hat{M}^{(XL)}_K$ represents the transition electromagnetic operator of type X with multipolarity L and its projection K. Γ is the width of the local Lorentzian energy spread of each solution of the QRPA equation which takes into account two and more phonon components and/or escape widths into a continuum. The excitation-energy-independent width $\Gamma = 1$ MeV was adopted for all XL for results presented in the paper, although some tests with both smaller and larger widths were made. Different Γ have never lead to a better description of the experimental spectra.

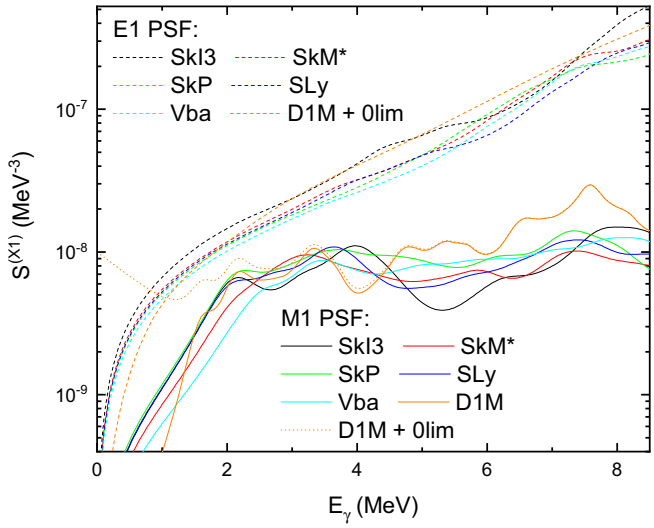

FIG. 14. PSFs from QRPA models. Lorentzian folding using $\Gamma = 1$ MeV was applied to results with all Skyrme interaction parametrizations. Data for the D1M interaction are from Ref. [4]; the impact of $S_{0\text{lim}}$ is indicated.

The PSFs based of the QRPA calculations with different forms of the Skyrme effective interaction [52–54] were tested. Specifically, we employed the SkI3 [68], SkM* [69], SLy6 [70], Vba [71], and SkP [72] parametrizations. They reproduce similarly well global nuclear characteristics (binding energy, radii) but each of them was adjusted considering different quantities. As a result they cover a broad range of the incompressibility of nuclear matter and the effective nucleon mass [67]. In general, the outcomes of the QRPA calculations with Skyrme-type interactions describe reasonably the position (and above neutron separation energies also shape) of the GEDR [67] and predict substantial orbital $M1$ strength in the SM region [73], but the description of the SF $M1$ resonance region requires additional adjustments [73]. Note that in the energy region of the SM (3–4 MeV) the interference of the SM and the low-energy tail of the SF $M1$ resonance is large and cannot be neglected [54]. Deduced PSFs for all tested Skyrme-force parametrizations are shown in Fig. 14. The strict form of the Brink hypothesis was assumed while simulating the γ decay process.

TABLE III. Predicted quadrupole deformation β_2 and energy of the 4_1^- (isomeric) state, $E_{4_1^-}$, obtained with various Skyrme interaction parametrizations. Also shown is the energy shift Δ_E needed for reproduction of the experimental position of the SM.

Interaction	SkI3	SkM*	SLy6	Vba	SkP	Evaluation [17]
β_2	0.352	0.348	0.350	0.339	0.341	0.34
$E_{4_1^-}$ (keV)	1015	1053	1047	1416	1403	1094
Δ_E (MeV)	−0.8	0	−0.5	−0.3	−0.5	

An energy shift Δ_E is often applied to the excitation energies from QRPA calculations to match them with experimental data. This is, for instance, the case of the PSF model based on the QRPA+D1M calculations from review [4]. We thus also tested PSFs based on calculated strengths shifted by Δ_E, applied in $S^{(M1)}$; no shift was applied to $S^{(E1)}$. This shift moved the centroid of the strongest predicted bump in $S^{(M1)}$ to $E_\gamma \approx 3.2$ MeV; the reason for this shift is discussed throughout Sec. IV. The applied Δ_E is indicated in Table III.

As described in Sec. IV A, the PSF model based on the QRPA+D1M calculations from review [4] features an empirical low-energy PSF part $S_{0\text{lim}}$. We also checked the impact of adding the same $S_{0\text{lim}}$ also to calculations with the Skyrme interaction parametrizations.

Table III gives tested shift Δ_E as well as the equilibrium quadrupole deformation β_2 obtained from the minimum of the quasiparticle mean field energy for each parametrization. To indicate the quality of individual parametrizations we also show predicted the energy of the first (isomeric) $I^\pi K = 4^-4$ state, observed experimentally at 1094 keV; SkI3, SkM, and SLy6 predict the energy quite well, while Vba and SkP are off by about 400 keV. The best agreement of calculated $E_{4_1^-}$ with experiment was obtained for parametrizations with low values of effective nucleon mass ($m^*/m = 0.58$, 0.79, and 0.69 for SkI3, SkM*, and Sly6, respectively).

[1] M. Arnould and S. Goriely, Prog. Part. Nucl. Phys. **112**, 103766 (2020).
[2] J. J. Cowan, C. Sneden, J. E. Lawler, A. Aprahamian, M. Wiescher, K. Langanke, G. Martínez-Pinedo, and F.-K. Thielemann, Rev. Mod. Phys. **93**, 015002 (2021).
[3] U.S. DOE Office of Science, Report of the Nuclear Physics and Related Computational Science R&D for Advanced Fuel Cycles Workshop, August 10–12, 2006, Bethesda, MD, 2006 (OSTI, 2006), https://www.osti.gov/servlets/purl/1298979.
[4] S. Goriely, P. Dimitriou, M. Wiedeking, T. Belgya, R. Firestone, J. Kopecky, M. Krtička, V. Plujko, R. Schwengner, S. Siem, H. Utsunomiya, S. Hilaire, S. Peru, Y. S. Cho, D. M. Filipescu, N. Iwamoto, T. Kawano, V. Varlamov, and R. Xu, Eur. Phys. J. A **55**, 172 (2019).
[5] R. Capote, M. Herman, P. Obložinský, P. G. Young, S. Goriely, T. Belgya, A. V. Ignatyuk, A. J. Koning, S. Hilaire, V. A. Plujko, M. Avrigeanu, O. Bersillon, M. B. Chadwick, T. Fukahori, Z. Ge, Y. Han, S. Kailas, J. Kopecky, V. M. Maslov, G. Reffo *et al.*, Nucl. Data Sheets **110**, 3107 (2009).
[6] R. R. Hilton, Proceedings of the International Conference on Nuclear Structure, Dubna, 1976 (unpublished).
[7] N. Iudice and F. Palumbo, Phys. Rev. Lett. **41**, 1532 (1978).
[8] A. Chyzh, B. Baramsai, J. A. Becker, F. Bečvář, T. A. Bredeweg, A. J. Couture, D. Dashdorj, R. C. Haight, M. Jandel, J. Kroll, M. Krtička, G. E. Mitchell, J. M. O'Donnell, W. Parker, R. S. Rundberg, J. L. Ullmann, D. J. Vieira, C. L. Walker, J. B. Wilhelmy, J. M. Wouters *et al.*, Phys. Rev. C **84**, 014306 (2011).

[9] B. Baramsai, J. Kroll, G. E. Mitchell, U. Agvaanluvsan, F. Bečvář, T. A. Bredeweg, A. Chyzh, A. J. Couture, D. Dashdorj, R. C. Haight, M. Jandel, A. L. Keksis, M. Krtička, J. M. O'Donnell, R. S. Rundberg, J. L. Ullmann, D. J. Vieira, and C. L. Walker, Phys. Rev. C **87**, 044609 (2013).

[10] S. Valenta, B. Baramsai, T. A. Bredeweg, A. J. Couture, A. Chyzh, M. Jandel, J. Kroll, M. Krtička, G. E. Mitchell, J. M. O'Donnell, G. Rusev, J. L. Ullmann, and C. L. Walker, Phys. Rev. C **96**, 054315 (2017).

[11] H. T. Nyhus, S. Siem, M. Guttormsen, A. C. Larsen, A. Bürger, N. U. H. Syed, G. M. Tveten, and A. Voinov, Phys. Rev. C **81**, 024325 (2010); **82**, 029909(E) (2010).

[12] E. Melby, M. Guttormsen, J. Rekstad, A. Schiller, S. Siem, and A. Voinov, Phys. Rev. C **63**, 044309 (2001).

[13] A. C. Larsen, M. Guttormsen, M. Krtička, E. Běták, A. Bürger, A. Görgen, H. T. Nyhus, J. Rekstad, A. Schiller, S. Siem, H. K. Toft, G. M. Tveten, A. V. Voinov, and K. Wikan, Phys. Rev. C **83**, 034315 (2011); **97**, 049901(E) (2018).

[14] U. Kneissl, H. H. Pitz, and A. Zilges, Prog. Part. Nucl. Phys. **37**, 349 (1996).

[15] W. F. Davidson, D. D. Warner, R. F. Casten, K. Schreckenbach, H. G. Borner, J. Simic, M. Stojanovic, M. Bogdanovic, S. Koicki, W. Gelletly, G. B. Orr, and M. L. Stelts, J. Phys. G **7**, 455 (1981).

[16] A. Jungclaus, R. F. Casten, R. L. Gill, and H. G. Börner, Phys. Rev. C **49**, 88 (1994).

[17] C. M. Baglin, Nucl. Data Sheets **111**, 1807 (2010).

[18] K. Wisshak, F. Voss, F. Käppeler, L. Kazakov, F. Bečvář, M. Krtička, R. Gallino, and M. Pignatari, Phys. Rev. C **73**, 045807 (2006).

[19] X. Ledoux, J. Sigaud, T. Granier, J.-P. Lochard, Y. Patin, P. Pras, C. Varignon, J.-M. Laborie, Y. Boulin, and F. Gunsing, Eur. Phys. J. A **27**, 59 (2006).

[20] D. Denis-Petit, O. Roig, V. Méot, B. Morillon, P. Romain, M. Jandel, T. Kawano, D. J. Vieira, E. M. Bond, T. A. Bredeweg, A. J. Couture, R. C. Haight, A. L. Keksis, R. S. Rundberg, and J. L. Ullmann, Phys. Rev. C **94**, 054612 (2016).

[21] M. Heil, R. Reifarth, M. M. Fowler, R. C. Haight, F. Käppeler, R. S. Rundberg, E. H. Seabury, J. L. Ullmann, and K. Wisshak, Nucl. Instrum. Methods Phys. Res., Sect. A **459**, 229 (2001).

[22] R. Reifarth, T. A. Bredeweg, A. Alpizar-Vicente, J. C. Browne, E.-I. Esch, U. Greife, R. C. Haight, R. Hatarik, A. Kronenberg, J. M. O'Donnell, R. S. Rundberg, J. L. Ullmann, D. J. Vieira, J. B. Wilhelmy, and J. M. Wouters, Nucl. Instrum. Methods Phys. Res., Sect. A **531**, 530 (2004).

[23] P. W. Lisowski, C. D. Bowman, G. J. Russell, and S. A. Wender, Nucl. Sci. Eng. **106**, 208 (1990).

[24] M. Mocko and G. Muhrer, Nucl. Instrum. Methods Phys. Res., Sect. A **704**, 27 (2013).

[25] M. Jandel, T. A. Bredeweg, A. J. Couture, M. M. Fowler, E. M. Bond, M. B. Chadwick, R. R. C. Clement, E.-I. Esch, J. M. O'Donnell, R. Reifarth, R. S. Rundberg, J. L. Ullmann, D. J. Vieira, J. B. Wilhelmy, J. M. Wouters, R. A. Macri, C. Y. Wu, and J. A. Becker, Nucl. Instrum. Methods B **261**, 1117 (2007).

[26] S. Mosby, A. J. Couture, M. Jandel, and J. M. O'Donnell, Los Alamos National Laboratory Report No. LA-UR-18-22130, 2018 (unpublished).

[27] S. F. Mughabghab, *Atlas of Neutron Resonances, Volume 2: Resonance Properties and Thermal Cross Sections Z=61-102* (Elsevier, Amsterdam, 2018).

[28] I. Knapová, S. Valenta, B. Baramsai, T. A. Bredeweg, A. Couture, C. Fry, M. Jandel, J. Kroll, M. Krtička, G. E. Mitchell, J. M. O'Donnell, C. J. Prokop, G. Rusev, and J. L. Ullmann, Phys. Rev. C **106**, 034607 (2022).

[29] S. Valenta, Study of statistical decay in well deformed rare-earth nuclei, Ph.D. thesis, Charles University, 2018, http://hdl.handle.net/20.500.11956/102486.

[30] N. Simbirtseva, M. Krtička, R. F. Casten, A. Couture, W. I. Furman, I. Knapová, J. M. O'Donnell, G. Rusev, J. L. Ullmann, and S. Valenta, Phys. Rev. C **101**, 024302 (2020).

[31] I. Knapová, Study of gamma decay in ^{168}Er from neutron capture, Ph.D. thesis, Charles University, Prague, 2022, http://hdl.handle.net/20.500.11956/177739.

[32] F. Bečvář, Nucl. Instrum. Methods Phys. Res., Sect. A **417**, 434 (1998); **935**, 240 (2019).

[33] M. Krtička and S. Valenta, https://www-nds.iaea.org/dicebox/ (2018).

[34] S. Agostinelli *et al.*, Nucl. Instrum. Methods Phys. Res., Sect. A **506**, 250 (2003).

[35] C. E. Porter and R. G. Thomas, Phys. Rev. **104**, 483 (1956).

[36] T. von Egidy and D. Bucurescu, Phys. Rev. C **72**, 044311 (2005); **73**, 049901(E) (2006).

[37] T. von Egidy and D. Bucurescu, Phys. Rev. C **80**, 054310 (2009).

[38] S. I. Al-Quraishi, S. M. Grimes, T. N. Massey, and D. A. Resler, Phys. Rev. C **67**, 015803 (2003).

[39] T. von Egidy and D. Bucurescu, Phys. Rev. C **78**, 051301(R) (2008).

[40] A. Koning, S. Hilaire, and S. Goriely, Nucl. Phys. A **810**, 13 (2008).

[41] S. Goriely, S. Hilaire, and A. J. Koning, Phys. Rev. C **78**, 064307 (2008).

[42] S. S. Dietrich and B. L. Berman, At. Data Nucl. Data Tables **38**, 199 (1988).

[43] T. Kawano, Y. S. Cho, P. Dimitriou, D. Filipescu, N. Iwamoto, V. Plujko, X. Tao, H. Utsunomiya, V. Varlamov, R. Xu, R. Capote, I. Gheorghe, O. Gorbachenko, Y. L. Jin, T. Renstrom, M. Sin, K. Stopani, Y. Tian, G. M. Tveten, J. M. Wang *et al.*, Nucl. Data Sheets **163**, 109 (2020).

[44] D. M. Brink, Some aspect of the interaction of fields with matter, Ph.D. thesis, Oxford University, 1955 (unpublished).

[45] S. G. Kadmenskii, V. P. Markushev, and V. I. Furman, Sov. J. Nucl. Phys **37**, 165 (1983).

[46] M. Guttormsen, A. Bagheri, R. Chankova, J. Rekstad, S. Siem, A. Schiller, and A. Voinov, Phys. Rev. C **68**, 064306 (2003).

[47] S. Valenta, F. Bečvář, J. Kroll, M. Krtička, and I. Tomandl, Phys. Rev. C **92**, 064321 (2015).

[48] J. Kroll, B. Baramsai, G. E. Mitchell, U. Agvaanluvsan, F. Bečvář, T. A. Bredeweg, A. Chyzh, A. J. Couture, D. Dashdorj, R. C. Haight, M. Jandel, A. L. Keksis, M. Krtička, J. M. O'Donnell, W. Parker, R. S. Rundberg, J. L. Ullmann, S. Valenta, D. J. Vieira, C. Walker *et al.*, Phys. Rev. C **88**, 034317 (2013).

[49] R. E. Chrien, in *Proceedings of the 5th International School on Neutron Physics*, Alushta, USSR, 1987, edited by B. B. Kolesova and V. R. Sarantseva, JINR Report No. D3,4,17-86-747 (JINR, Dubna, 1987).

[50] J. Kopecky, M. Uhl, and R. E. Chrien, Phys. Rev. C **47**, 312 (1993).

[51] S. Goriely, S. Hilaire, S. Péru, and K. Sieja, Phys. Rev. C **98**, 014327 (2018).

[52] A. Repko, J. Kvasil, V. O. Nesterenko, and P.-G. Reinhard, Eur. Phys. J. A **53**, 221 (2017).
[53] J. Kvasil, A. Repko, and V. O. Nesterenko, Eur. Phys. J. A **55**, 213 (2019).
[54] V. O. Nesterenko, P. I. Vishnevskiy, J. Kvasil, A. Repko, and W. Kleinig, Phys. Rev. C **103**, 064313 (2021).
[55] F. Iachello, Nucl. Phys. A **358**, 89 (1981).
[56] D. Bohle, A. Richter, W. Steffen, A. E. L. Dieperink, N. Lo Iudice, F. Palumbo, and O. Scholten, Phys. Lett. B **137**, 27 (1984).
[57] D. Bohle, G. Küchler, A. Richter, and W. Steffen, Phys. Lett. B **148**, 260 (1984).
[58] H. Maser, S. Lindenstruth, I. Bauske, O. Beck, P. von Brentano, T. Eckert, H. Friedrichs, R. D. Heil, R.-D. Herzberg, A. Jung, U. Kneissl, J. Margraf, N. Pietralla, H. H. Pitz, C. Wesselborg, and A. Zilges, Phys. Rev. C **53**, 2749 (1996).
[59] M. Krtička, F. Bečvář, J. Honzátko, I. Tomandl, M. Heil, F. Käppeler, R. Reifarth, F. Voss, and K. Wisshak, Phys. Rev. Lett. **92**, 172501 (2004).
[60] A. Voinov, M. Guttormsen, E. Melby, J. Rekstad, A. Schiller, and S. Siem, Phys. Rev. C **63**, 044313 (2001).
[61] D. Frekers, H. Wörtche, A. Richter, R. Abegg, R. Azuma, A. Celler, C. Chan, T. Drake, R. Helmer, K. Jackson, J. King, C. Miller, R. Schubank, M. Vetterli, and S. Yen, Phys. Lett. B **244**, 178 (1990).
[62] A. Simon, M. Guttormsen, A. C. Larsen, C. W. Beausang, P. Humby, J. T. Harke, R. J. Casperson, R. O. Hughes, T. J. Ross, J. M. Allmond, R. Chyzh, M. Dag, J. Koglin, E. McCleskey, M. McCleskey, S. Ota, and A. Saastamoinen, Phys. Rev. C **93**, 034303 (2016).
[63] G. M. Gurevich, L. E. Lazareva, V. M. Mazur, S. Y. Merkulov, G. V. Solodukhov, and V. A. Tyutin, Nucl. Phys. A **351**, 257 (1981).
[64] T. Renstrøm, H. Utsunomiya, H. T. Nyhus, A. C. Larsen, M. Guttormsen, G. M. Tveten, D. M. Filipescu, I. Gheorghe, S. Goriely, S. Hilaire, Y.-W. Lui, J. E. Midtbø, S. Péru, T. Shima, S. Siem, and O. Tesileanu, Phys. Rev. C **98**, 054310 (2018).
[65] W. F. Davidson and W. R. Dixon, J. Phys. G: Nucl. Part. Phys. **17**, 1683 (1991).
[66] H. D. Choi, R. B. Firestone, R. M. Lindstrom, G. L. Molnar, S. F. Mughabghab, R. Paviotti Corcuera, Z. Revay, A. Trkov, V. Zerkin, and C. Zhou, Database of Prompt Gamma Rays from Slow Neutron Capture for Elemental Analysis, Technical Report No. IAEA-STI/PUB/1263 2007 (IAEA, Vienna, 2007).
[67] W. Kleinig, V. O. Nesterenko, J. Kvasil, P.-G. Reinhard, and P. Veselý, Phys. Rev. C **78**, 044313 (2008).
[68] P. Reinhard and H. Flocard, Nucl. Phys. A **584**, 467 (1995).
[69] J. Bartel, P. Quentin, M. Brack, C. Guet, and H. Hakansson, Nucl. Phys. A **386**, 79 (1982).
[70] E. Chabanat, P. Bonche, P. Haensel, J. Meyer, and R. Schaeffer, Nucl. Phys. A **635**, 231 (1998).
[71] P. Klüpfel, P.-G. Reinhard, T. J. Burvenich, and J. A. Maruhn, Phys. Rev. C **79**, 034310 (2009).
[72] P. G. Reinhard, D. J. Dean, W. Nazarewicz, J. Dobaczewski, J. A. Maruhn, and M. R. Strayer, Phys. Rev. C **60**, 014316 (1999).
[73] V. O. Nesterenko, J. Kvasil, P. Veselý, W. Kleinig, P.-G. Reinhard, and V. Y. Ponomarev, J. Phys. G: Nucl. Part. Phys. **37**, 064034 (2010).